THE ASTROPHYSICAL JOURNAL, 516:843–862, 1999 May 10

DYNAMICAL EVOLUTION AND IONIZATION STRUCTURE OF AN EXPANDING SUPERBUBBLE: APPLICATION TO W4

SHANTANU BASU, DOUG JOHNSTONE, AND P. G. MARTIN
Canadian Institute for Theoretical Astrophysics, University of Toronto, 60 Saint George Street, Toronto, Ontario M5S 3H8, Canada; basu, johnstone, pgmartin@cita.utoronto.ca
Received 1998 March 13; accepted 1998 December 14

ABSTRACT

Recent observations have revealed a superbubble associated with the young stellar cluster OCl 352 near the W4 H II region: a void in H I emission, reported by Normandeau and coworkers, and a bright shell in Hα emission, reported by Dennison and coworkers. We investigate the hypothesis that the bubble is blown by stellar winds from the O-type stars in the association. The Kompaneets approximation is adapted to model a wind-blown bubble in a stratified interstellar medium. We describe some general principles necessary for understanding the dynamics of an expanding bubble and the associated ionization structure in a stratified atmosphere. The Kompaneets model can be used to determine the mean scale height of the ambient medium as well as the age of the bubble. The ionization structure also places constraints on the ambient density near the cluster. We also estimate the surface brightness of the shell and the fraction of ionizing photons that escape the bubble. The prescription we use can be applied to any observed bubble that is blown by the effectively continuous energy output of stellar winds or multiple supernovae. Application to the W4 superbubble shows that the mean scale height of the ambient gas around the cluster is remarkably small, 25 pc for a cluster distance of 2.35 kpc. The age of the bubble is estimated to be about 2.5 Myr, consistent with the notion that the bubble is blown by stellar winds from a very young cluster in which no supernovae have yet occurred.

Subject headings: H II regions — ISM: bubbles — ISM: individual (W4 Supershell) — shock waves — supernova remnants

1. INTRODUCTION

Normandeau, Taylor, & Dewdney (1996, 1997, hereafter referred to collectively as NTD) have observed a large cavity in H I above the W4 H II region in the Pilot project of the arcminute resolution Canadian Galactic Plane Survey (CGPS). The conical cavity, found in the velocity range from $v_{\rm LSR} = -31.9$ to -46.7 km s^{-1}, opens upward above (and perpendicular to) the Galactic plane and is bounded below by the W4 H II region, which is part of the larger W3/W4/W5 H II region complex located in the Perseus arm of the outer Galaxy. Panoramic images of CO and thermal dust (*IRAS*) emission from this region, also at arcminute resolution, have been presented by Heyer & Terebey (1998). An association of nine O-type stars, part of the stellar cluster OCl 352 (also IC 1805), centered at $(l, b) = (134.^\circ7, 0.^\circ9)$, is situated near the base of the cavity, suggesting that the cavity has been created by outflows from these stars. Spectroscopic parallax (Massey, Johnson, & DeGioia-Eastwood 1995) places OCl 352 at a distance 2.35 kpc; at this distance, the H I cavity has a width $\simeq 110$ pc at a latitude $b \simeq 3.^\circ5$, or $\simeq 110$ pc above the cluster. Radio continuum data presented by NTD show the presence of a shell of ionized gas along the lower edge of the H I cavity. Dennison, Topasna, & Simonetti (1997, hereafter DTS) have observed the same region in Hα with a field of view extending to higher Galactic latitude. Their image shows that the H I cavity of NTD is located near the base of a highly elongated shell of Hα emission, which appears to close far above the Galactic plane. This shell is interpreted here to be the dense ionized wall of swept-up gas surrounding a bubble of hot rarefied gas created by the outflow from the massive stars.

This structure is one example of a vast collection of bubbles and associated shells that are thought to populate the interstellar medium (ISM) of galaxies. In our Galaxy, H I observations (Heiles 1979, 1984) reveal numerous shells with dimensions of several hundred pc. Other spiral, irregular, and dwarf galaxies also show evidence for shells and holes in H I (e.g., Brinks & Bajaja 1986; Deul & den Hartog 1990; Puche et al. 1992). The holes in H I may be sites where the bubbles have blown out of the stratified ISM and into the halo of the host galaxies. Norman & Ikeuchi (1989) suggest that these "chimneys" are a common feature in our Galaxy.

The well-resolved structure of the W4 superbubble and the well-known properties of the stellar cluster OCl 352 that drives the bubble afford us a chance to apply theoretical models to gain insight into the massive star–ISM interaction in a star-forming region of our Galaxy. We show that the highly elongated nature of the superbubble implies the presence of significant vertical stratification in the ambient ISM; the scale height is remarkably small.

Theoretical models of bubble expansion in a stratified medium come in many varieties. Kompaneets (1960) found a semianalytic solution for the expansion of a blast wave in an exponential atmosphere. The Kompaneets approximation assumes the following: (1) uniform pressure within the bubble, (2) bubble expansion in a direction normal to the local surface, and (3) expansion speed implied by a strong shock (i.e., the internal pressure dominates the external pressure). Kompaneets found an analytic expression for the shape of the bubble during its expansion. The time-evolution of the bubble can be found by numerical integration. The Kompaneets solution has been used and adapted for application to various astrophysical phenomena, including relativistic blast waves (Shapiro 1979), active galaxy winds (Schiano 1985), and impacts within the deep gaseous envelopes of giant planets (Korycansky 1992). More sophis-

ticated models of bubble expansion include the thin-shell approximation (MacLow & McCray 1988; Bisnovatyi-Kogan, Blinnikov, & Silich 1989), which employs the first two assumptions of the Kompaneets approximation but determines the expansion speed through direct numerical integration of the momentum equation for various segments of the thin shell of swept-up gas. This numerical approach accounts for the inertia of the swept-up shell, and external pressure and gravity can also be included. Finally, full numerical integration of the hydrodynamic equations (e.g., Tomisaka & Ikeuchi 1986; MacLow, McCray, & Norman 1989; Tenorio-Tagle, Rozyczka, & Bodenheimer 1990) and magnetohydrodynamic equations (Tomisaka 1992, 1998) yield the most complete solutions to date. For a review of models of bubble expansion in the ISM, see Bisnovatyi-Kogan & Silich (1995).

In this paper, we choose to apply the Kompaneets model because, in addition to its simplicity, the semianalytic solution allows a more direct insight into the physics of bubble expansion. An observed bubble can be matched to theory using analytic expressions, yielding straightforward estimates of the atmospheric structure and bubble age. The original Kompaneets model is adapted so that the energy input is continuous rather than occurring at an initial instant, as is expected with stellar winds or multiple sequential supernovae. We discuss the conditions under which the Kompaneets solution is valid and show how some of its properties can be used in an analysis of observed bubbles. Application of the model to the W4 superbubble gives us a more accurate age estimate than is possible with models of spherical expansion, as well as a dynamical estimate of the gas scale height in the W4 star-forming region. Given the structure of the bubble and ambient atmosphere, we also illustrate the evolution of the ionized gas structure created by the O-type stars. The current structure of the ionized shell places an additional constraint on the mean density of the ambient atmosphere and allows predictions of how much ionizing flux escapes through the bubble.

The outline of this paper is as follows: In § 2 we apply the Kompaneets model to the structure and evolution of the wind-blown bubble. The complementary role of the ionizing UV flux from the massive stars is discussed in § 3. We interpret our results in § 4, and a summary of our main conclusions is given in § 5. Readers who wish to review a more complete exposition of the Kompaneets solution are referred to the Appendix.

2. DYNAMICAL EVOLUTION OF A SUPERBUBBLE

2.1. *Early Evolution and Blowout Condition*

The early evolution of a superbubble in a stratified medium can be described by the model for spherical expansion of a stellar-wind bubble in a homogeneous medium, as developed by Castor, McCray, & Weaver (1975) and Weaver et al. (1977). Their model can be applied to bubbles powered by the combined winds of several O and B stars if they are closely associated and can even apply to bubbles powered by multiple sequential supernovae from such an association, since the energy output is effectively continuous (McCray & Kafatos 1987; MacLow & McCray 1988). We briefly describe the model of Castor et al. (1975) and Weaver et al. (1977) before proceeding to discuss the effects of vertical stratification.

The earliest phase is one of free expansion of the wind, which drives a shock front into the ambient ISM. A shell of swept-up ISM is formed behind the shock front, and once its inertia slows down the shell appreciably, an inner shock front is also formed. This inner shock slows down the hypersonic free wind before it encounters the more slowly moving shell, creating a region of hot, shocked wind gas. Hence most of the bubble evolution is characterized by a four-zone structure: (1) an innermost freely expanding stellar wind surrounded by the inner shock surface; (2) a hot, almost isobaric region consisting of shocked wind gas and a small fraction of swept-up ISM gas; (3) a shell of swept-up ISM gas separated from region 2 by a contact discontinuity; and (4) the undisturbed ISM, separated from region 3 by the outer shock front. Radiative cooling causes region 3 to collapse into a thin, dense shell within a few thousand years, while cooling remains relatively unimportant in the rarefied region 2. The inner shock front radius R_1 is found to be much smaller than the outer shock front radius R_2. Hence the expansion of the bubble can be modeled effectively as that of a thin-shell driven into the ambient medium with uniform density ρ_0 by an isobaric bubble of radius $R_s = R_2$. The internal energy of the bubble $E_{\rm th}$ (and hence the mean pressure P) is determined by the energy input from the luminosity L_0 of the wind minus the work done in expanding the bubble. Under these conditions, Castor et al. (1975) find the analytic solution

$$R_s = \left(\frac{125}{154\pi}\right)^{1/5} L_0^{1/5}\ \rho_0^{-1/5}\ t^{3/5}\,, \tag{1}$$

$$E_{\rm th} = \frac{5}{11} L_0\, t\,, \tag{2}$$

$$P = \frac{2}{3}\frac{E_{\rm th}}{\Omega} = \frac{7}{(3850\pi)^{2/5}}\ L_0^{2/5}\ \rho_0^{3/5}\ t^{-4/5}\,, \tag{3}$$

where $\Omega = 4\pi R_s^3/3$ is the volume of the bubble and a ratio of specific heats $\gamma = \frac{5}{3}$ has been used for the equation of state in the bubble interior. The expansion will dissipate and the shell will begin to merge with the ISM when the expansion speed $u = \frac{3}{5}R_s/t$ ($\propto t^{-2/5}$) decreases to the sound speed of the external medium $c_{s,e} = (P_e/\rho_0)^{1/2}$, where P_e is the external pressure (essentially the same time that $P = P_e$). This occurs at the stalling radius

$$R_{\rm stall} = \left(\frac{27}{154\pi}\right)^{1/2} L_0^{1/2}\, \rho_0^{1/4}\, P_e^{-3/4}\,. \tag{4}$$

In a stratified medium, $R_{\rm stall}$ is crucial in determining whether a bubble will "blow out." In such a medium, the initial expansion will be spherical, as in a homogeneous atmosphere. However, if the expansion does not stall before proceeding beyond one scale height H of an exponential atmosphere, then it will sense the stratification, and the top of the shell will begin to accelerate and reach an infinite height in a finite time, which defines blowout. Hence the dimensionless ratio $b = R_{\rm stall}/H$ is an important diagnostic for bubbles in a stratified medium; we surmise that $b \gtrsim 1$ for blowout to occur. Indeed, MacLow & McCray (1988) find a similar dimensionless ratio D, which gauges whether or not their bubbles blow out of a finite pressure exponential medium. Their parameter D can be written in our terminology as

$$D = \left(\frac{154\pi}{27}\right) b^2 = 17.9 b^2 \ . \tag{5}$$

MacLow & McCray (1988) find that a model with $D = 10$ ($b = 0.75$) is confined, but one with $D = 100$ ($b = 2.4$) blows out of the atmosphere, consistent with our expectation that blowout occurs for $b \gtrsim 1$.

In the case of the W4 superbubble, which can be blown by stellar winds alone, the estimated wind luminosity of the driving cluster OCl 352 is $L_0 = 3 \times 10^{37}$ ergs s^{-1} (NTD). Hence, for this bubble, equation (4) gives

$$b = 4 \left(\frac{L_0}{3 \times 10^{37} \text{ ergs s}^{-1}}\right)^{1/2} \left(\frac{n_0}{1 \text{ cm}^{-3}}\right)^{1/4} \times \left(\frac{10^4 \text{ cm}^{-3} \text{ K}}{P_e/k}\right)^{3/4} \left(\frac{100 \text{ pc}}{H}\right), \tag{6}$$

so that any standard interstellar values for n_0, P_e, and H will yield $b > 1$. In the W4 region, probably $b \gg 1$, since the scale height H is actually much less than 100 pc (see § 2), and the ambient density n_0 is actually greater than 1 cm^{-3} (see § 3). Our adopted normalizing value of P_e/k also represents the high end of estimated pressures in the ISM (Kulkarni & Heiles 1987).

2.2. *Expansion in a Stratified Atmosphere: Application to W4*

Kompaneets (1960) developed a semianalytic solution for shock wave propagation in an exponential atmosphere. This solution was originally used to study blast wave propagation, but we adapt it to include a continuous input of energy, as is also done by Schiano (1985) in his study of active galaxy winds. The model gives a good idea of how shock waves propagate in a stratified medium without having to solve the full hydrodynamic equations numerically. The shape of the bubble is determined analytically, and the time evolution is determined by integrating a differential equation. The spatial and temporal solutions of the Kompaneets model for a wind-blown bubble are presented in Appendix A. In the following sections, we apply the solution to the W4 superbubble.

2.2.1. *Relation of the Spatial Profiles to the W4 Superbubble*

Figure 1 shows the surface of the shock front $r(z, y)$ (eq. [A8]) for various values of the dimensionless quantity $\tilde{y} = y/H$, which parametrizes the evolution of the bubble (see § A.1). The shock surface is spherical at early times but becomes increasingly elongated in the vertical direction after the top surface has moved beyond one scale height. Several streamlines of the flow are represented by dashed lines. The elongated bubbles exhibit a striking resemblance to the observed W4 superbubble in the region above the star cluster. Figure 2 shows an H I map of NTD, and Figure 3 shows the Hα map of DTS, both overlaid with the best-fit Kompaneets model, determined as follows: The best fit is determined by finding the value of $\tilde{y}$ [in the full range (0, 2)] for which the aspect ratio matches that of the observed superbubble. The Hα map of DTS reveals the ionized wall of the superbubble and shows that it reaches a maximum diameter of 3.°6 at latitude 4° and thereafter starts to close. Figure 3 shows that there is a left-right asymmetry in the structure of the Hα shell. The maximum radius of the shell, measured relative to the longitude of the cluster (134.°7), is greater toward the right (2.°1) than toward the left (1.°5);

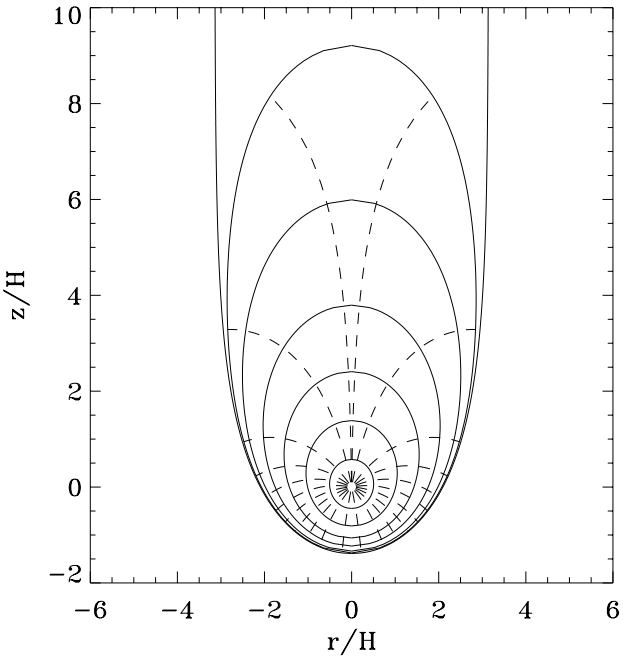

FIG. 1.—Evolution of the shock front in the Kompaneets solution, as the bubble expands in an exponential atmosphere $\rho = \rho_0 \exp(-z/H)$ and eventually blows out. Solid lines show the position of the shock front at seven successive times characterized by increasing values of the dimensionless parameter $\tilde{y}$ (=0.5, 1.0, 1.4, 1.7, 1.9, 1.98, and 2.0). Dashed lines show the streamlines of the flow for various points along the shock front.

also, the shell is brighter toward the left. This is consistent with the interpretation that the bubble has blown into a denser medium on the left side, so that it has not expanded as far. When ionization bounded (see § 3.2), a shell is brighter when closer to the cluster. A slightly lower density toward the right-hand side may also explain why the shell appears to extend to somewhat greater height on that side. Since our intention is to model the mean atmosphere, and not such details as a left-right asymmetry, we take an average value of 1.°8 for the maximum radius, thereby finding the Kompaneets model whose diameter matches that of the superbubble. In the same spirit, the top of the shell, while not clearly visible in the Hα map, is estimated to be at latitude 6.°9, based on the shell structure on both left and right. The star cluster is located at 0.°9 latitude. Using this information, equations (A9) and (A10), which give expressions for z_1 (z_2), the distance from the star cluster to the top (bottom) of the bubble, and $r_{\max}$, the maximum half-width of the bubble, are used to find the evolutionary stage of the bubble. Equating the theoretical and observed aspect ratios yields

$$\frac{z_1}{r_{\max}} = -\frac{\ln(1 - \tilde{y}/2)}{\arcsin(\tilde{y}/2)} \simeq \frac{6}{1.8} = 3.33 \ . \tag{7}$$

The equality is satisfied when $\tilde{y} = 1.9837$. In this calculation, we have assumed that the superbubble lies in a plane perpendicular to our line of sight. Our value of $\tilde{y}$ is also consistent with the location of the bottom of the bubble, since the Kompaneets model predicts that $|z_2|/z_1 = 0.14$ when $\tilde{y} = 1.9837$, whereas the observations yield $|z_2|/z_1 = 0.15$. The purely exponential atmosphere might be less realistic below the cluster, and finite external pressure might play a role there if anywhere, so it is fortunate that the

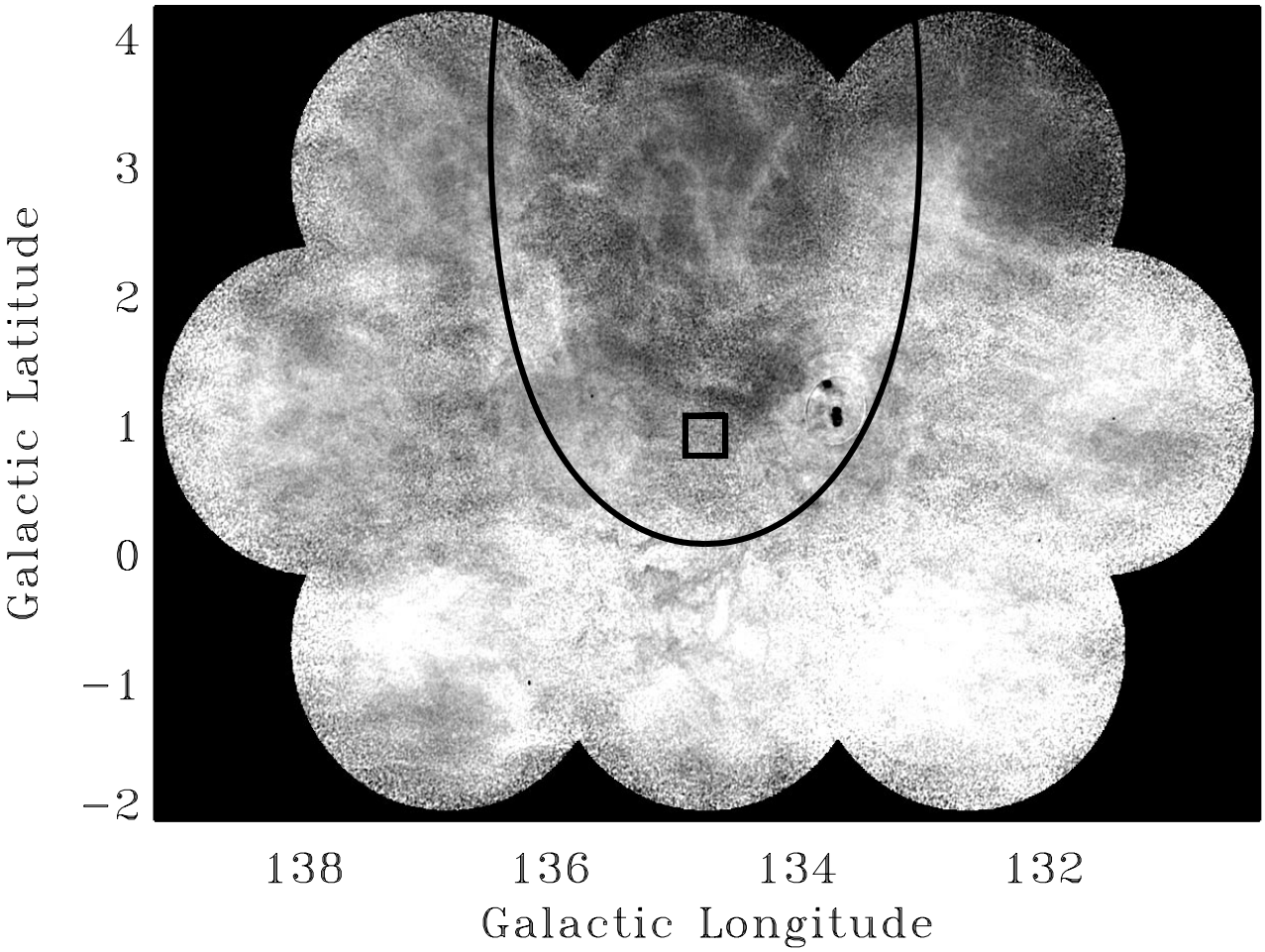

FIG. 2.—H I channel map showing the location of neutral hydrogen in the vicinity of W4 and revealing the empty chimney discovered by NTD97. Lighter shadings correspond to brighter H I emission. Overlaid on the figure is a Kompaneets solution with $\tilde{y} = 1.98$ and $H = 25$ pc, centered on the star cluster OCl 352.

model approximately fits the bubble here as well (see § 4 for further discussion of the physics near the base of the bubble).

In addition to matching the aspect ratio, the Kompaneets model also yields a value for the mean scale height H in the atmosphere if we know the size of the superbubble. This requires a distance, which we take to be 2.35 kpc, based on the distance to OCl 352 estimated by Massey et al. (1995). At this distance, the Hα map yields $z_1 \simeq 246$ pc and $r_{\max} \simeq 74$ pc. Since $\tilde{y} = 1.9837$ in the Kompaneets model implies that $z_1 = 9.62\ H$ and $r_{\max} = 2.89\ H$, matching the Kompaneets model to the observations requires

$$H \simeq 25 \text{ pc} . \tag{8}$$

Even though the exact position of z_1 is not very clear in the Hα map, the unmistakable presence of a maximum radius $r_{\max}$ alone can be used to obtain a rough estimate for H, since the highly elongated nature of the bubble implies that $r_{\max}$ ($\simeq 74$ pc) must be close to the limiting theoretical value πH. Furthermore, although our estimate for H is based on the Kompaneets model, it is worth pointing out that a scale height of this approximate magnitude is unavoidable in any model, since the current radius of the bubble (maximum value $\simeq 74$ pc) must be significantly greater than H in order for the bubble to have become so elongated.

2.2.2. *The Swept-up Mass in the Shell*

The mass distribution in the shell is an important factor in determining the ionization structure of the atmosphere, which is calculated in § 3. The spatial profiles can be used to find the streamlines of the flow, since the latter are normal to the local surface at all stages of evolution (see Fig. 1). Subsequently, one can integrate along the streamlines in the exponential atmosphere to obtain the swept-up surface (column) density at all points on the shell. Figure 4 shows the dimensionless surface density of the swept-up shell $\tilde{N}$ (unit $n_0 H$) when $\tilde{y} = 1.98$ (the stage of evolution that fits the W4 superbubble) as a function of (1) height z/H and (2) elevation angle θ (in degrees) measured relative to the r-axis. The surface density of the Kompaneets shell is shown as a solid line; the dashed line represents the value for expansion along a straight-line path to the radius $s = (r^2 + z^2)^{1/2}$ through the same exponential atmosphere. At $\theta = 0°$, the radial (straight-line) expansion would yield a surface density $N_s = n_0\, r(z = 0)/3 \simeq 2n_0 H/3$, since $r(z = 0) \simeq 2H$ at the advanced stages of evolution of a Kompaneets bubble. The Kompaneets streamlines yield a lower N than radial expansion for all angles $\theta > 0°$, since the streamlines tend to be deflected downward and yield higher values for most angles $\theta < 0°$ for the same reason. The crossover between the two curves occurs just below $\theta = 0°$. At $\theta = 0°$, the Kompaneets

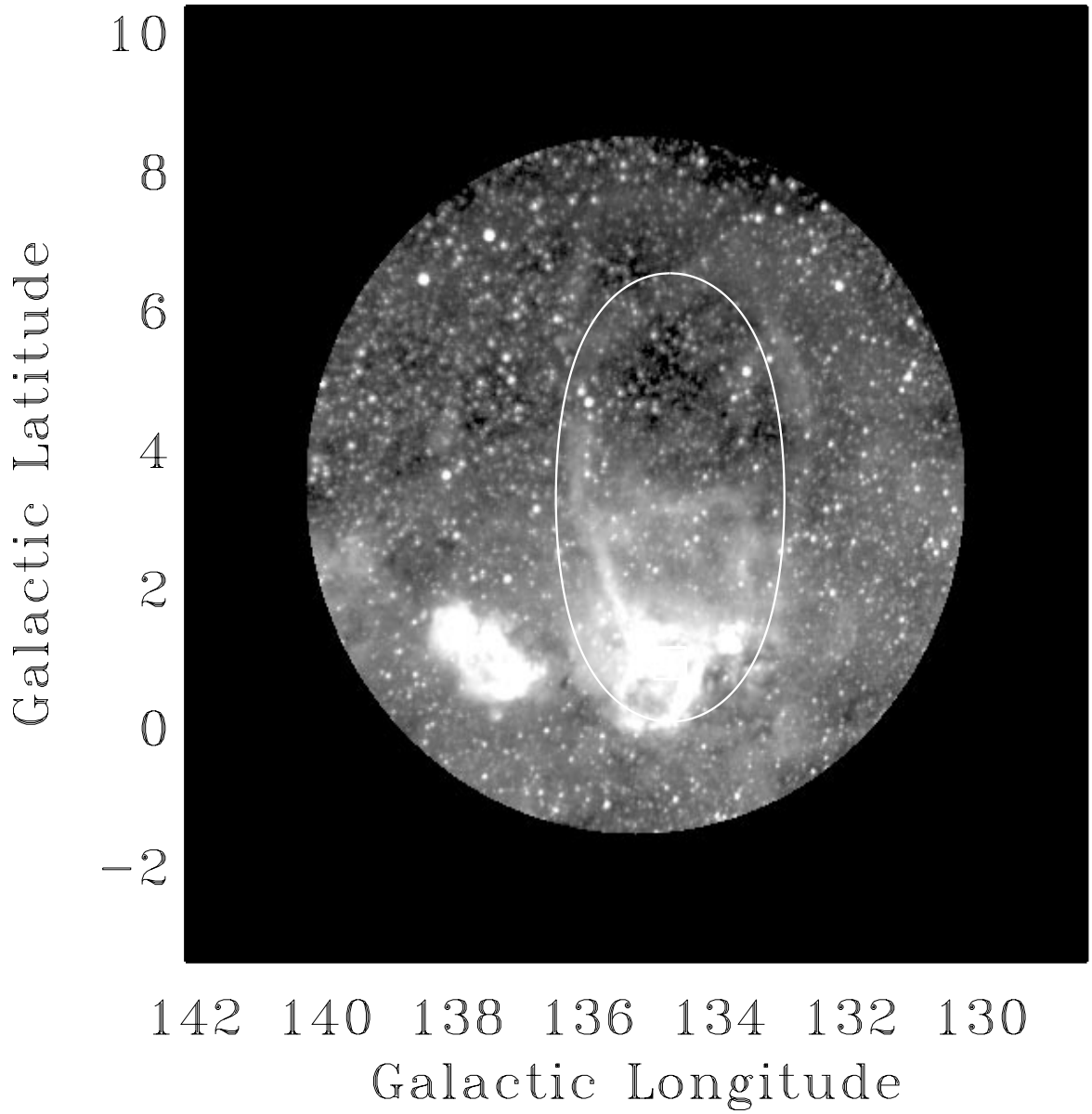

FIG. 3.—Hα map showing the location of ionized hydrogen in the vicinity of W4 and revealing the extended superbubble discovered by DTS. Lighter shadings correspond to brighter Hα emission. Overlaid is a Kompaneets solution with $\tilde{y} = 1.98$ and $H = 25$ pc, centered on the star cluster OCl 352, as in Fig. 2.

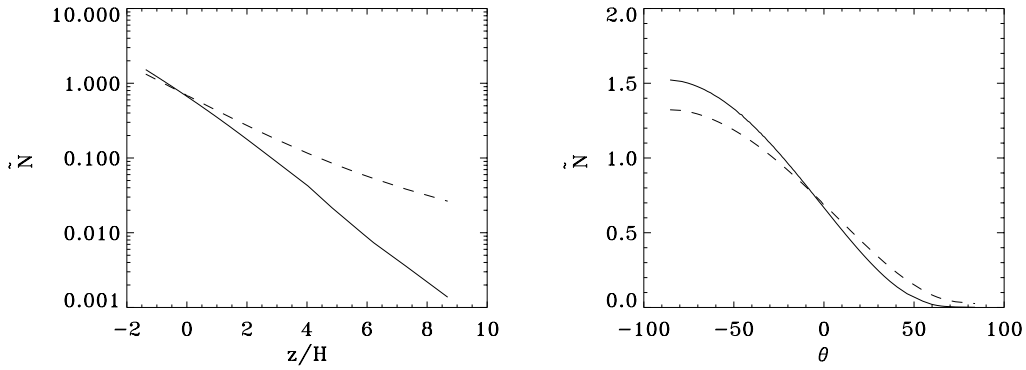

FIG. 4.—Surface density $\tilde{N}$ (unit $n_0 H$) in the swept-up shell, when $\tilde{y} = 1.98$, vs. height z/H (*left*) and angle θ (*right*), in degrees, measured relative to the r-axis ($z = 0$). The dashed line shows the surface density if the expansion had occurred along straight lines.

streamlines yield $N = 0.67 n_0 H$ versus $N_s = 0.69 n_0 H$ for radial streamlines. The Kompaneets streamlines yield values of N up to about 15% higher than the radial values near the bottom of the bubble. However, they are more than an order of magnitude below the radial values near the top. The continual downward deflection of streamlines means that most of the mass is not transported very far upward, if at all. In the late stages of the Kompaneets model, about 55% of the matter in the shell is found below $z = 0$, about 75% is found below $z = H$, and nearly 90% is found below $z = 2H$.

2.2.3. *Age of the W4 Superbubble*

The time-dependent solution (§ A.2) allows us to make an age estimate for any bubble if we know the stage of evolution (represented by $\tilde{y}$). For application to the W4 superbubble, we note that the dimensionless time $\tilde{t} = 6.3$ when $\tilde{y} = 1.98$. Converting to dimensional form, we obtain

$$t = 1.18 \left(\frac{n_0}{1 \text{ cm}^{-3}} \right)^{1/3} \left(\frac{H}{25 \text{ pc}} \right)^{5/3} \times \left(\frac{3 \times 10^{37} \text{ ergs s}^{-1}}{L_0} \right)^{1/3} \text{Myr} . \quad (9)$$

Although L_0 can be estimated from direct observations of the stellar winds in the cluster stars or from the spectral type of the stars (NTD), and H is estimated from the size and shape of the bubble, a final estimate for the bubble age requires a constraint on n_0, which we obtain in § 3 from the ionization structure of the atmosphere.

3. IONIZATION STRUCTURE

Along with the powerful winds that drive the W4 superbubble, the nine O stars also produce an extremely strong ultraviolet radiation field. The dynamics of the superbubble is dominated by the energetic winds, but the optical and radio continuum appearance of the region is determined by these ionizing photons.

The evolution of H II regions without powerful winds has been well studied (e.g., Spitzer 1978; Tenorio-Tagle 1982) and found to be incapable of producing extreme structures such as the W4 superbubble. The strongest constraint on dynamical H II regions is the inability to move large amounts of material at speeds much faster than the sound speed c_s in the hot, ionized gas of temperature $T \sim 10^4$ K. Unlike the wind-blown superbubble, where $T \sim 10^6$ K, an evolving H II region cannot expand more than a few tens of pc over its million year lifetime. The ionization structure of a wind-blown region is, however, produced by the irradiation of the swept-out cavity by the ionizing UV photons from the O stars. This allows observations of the ionized hydrogen to be used as a probe of the ambient atmospheric conditions.

3.1. *The Formation of* H II *Regions without Powerful Winds*

Before calculating the ionization structure of the wind-blown bubble, it is relevant to review the ionization structure of H II regions in a variety of media.

3.1.1. *Uniform Medium*

Within a constant density environment, the ionizing photon flux Φ_* from the central OB association produces a classical Strömgren sphere H II region with radius

$$R_{\text{St}} = \left(\frac{3\Phi_*}{4\pi n_0^2 \alpha_B} \right)^{1/3} . \quad (10)$$

In the above, n_0 is the number density of hydrogen nuclei inside the Strömgren sphere and $\alpha_B \simeq 2.6 \times 10^{-13}$ cm^3 s^{-1} is the recombination coefficient for hydrogen. For the nine O stars at the center of the W4 superbubble, $\Phi_* \simeq 2.3 \times 10^{50}$ s^{-1} (DTS), and the Strömgren radius is

$$R_{\text{St}} = 200 \left(\frac{1 \text{ cm}^{-3}}{n_0} \right)^{2/3} \left(\frac{\Phi_*}{10^{50} \text{ s}^{-1}} \right)^{1/3} \text{pc} . \quad (11)$$

Once formed, the initial H II region expands because of the overpressure of the hot, ionized gas relative to the external neutral gas.

3.1.2. *Exponentially Stratified Medium*

A second useful example to consider is the instantaneous structure of the initial H II region in an exponentially stratified atmosphere with scale height H. Because the density drops precipitously with increasing z, it is possible that in the upward direction the H II region will be unbounded. If H is much larger than R_{St}, so that the density gradient across the H II region is small, a quasi-spherical nebula is produced; however, if H is much smaller than R_{St}, the ionizing photons are free to escape the stratified ISM in the upward direction. Neglecting the diffuse ionizing field, the critical ratio $(R_{\text{St}}/H)_{\text{crit}}$ at which photons traveling directly upward can escape is found by equating the total number of recombinations within an infinitesimal solid angle $d\Omega$ in the z-direction with the UV flux Φ_*:

$$\Phi_* \frac{d\Omega}{4\pi} = \int_0^\infty n_0^2 \exp\left(\frac{-2z}{H} \right) \alpha_B z^2 \, dz \, d\Omega = \frac{1}{4} n_0^2 \alpha_B H^3 \, d\Omega . \quad (12)$$

Substituting equation (10) into equation (12) yields $(R_{\text{St}}/H)_{\text{crit}} = (3/4)^{1/3} \simeq 0.9$. Thus the condition for the initial Strömgren region to breakout is similar to that for the expansion of the wind-blown bubble; i.e., the characteristic radius must exceed the scale height.

Figure 5 plots the instantaneous ionization boundary for a variety of R_{St}/H values showing both confined and breakout H II regions. In each case, the boundary of the ionized region is calculated by equating photoionization and recombination along each solid angle. Note the gradual elongation of the nebula in the upward direction with increasing R_{St}/H and the shallow slope to the lower cavity when breakout is achieved. Like the initial Strömgren sphere in a uniform medium, these ionized regions represent the initial conditions for further dynamical evolution of the (overpressured) ionized gas. In extremely high-density (low R_{St}) or low scale height regions, the breakout solutions represent the initial conditions for champagne-flow H II regions (Tenorio-Tagle 1982), in which the ensuing dynamical evolution of the ionized gas at ~ 10 km s^{-1} is important.

When $R_{\text{St}}/H > 0.9$, a substantial fraction of the atmosphere above the OB association may be completely ionized, and a fraction of the ionizing photons may escape to the Galactic halo. The elevation angle θ_c above which photons escape to infinity is determined by evaluating an analogous relation to equation (12) along each solid angle (see also Franco, Tenorio-Tagle, & Bodenheimer 1990).

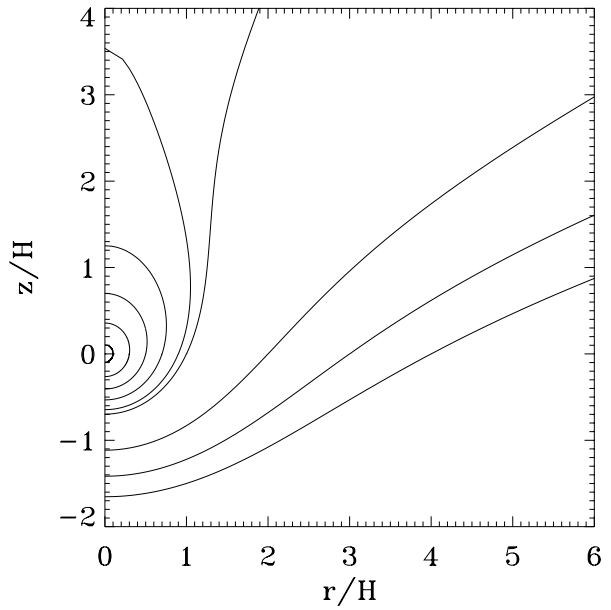

FIG. 5.—Location of the initial ionization front around an H II region formed within an exponential atmosphere. The computed models, from the innermost curve, are for $R_{St}/H =$ 0.1, 0.3, 0.5, 0.7, 0.9, 1.0, 2, 3, and 4.

This yields

$$\sin \theta_c = 0.9 \frac{H}{R_{St}} \quad \text{for} \quad \frac{R_{St}}{H} > 0.9 \, . \tag{13}$$

When $\theta_c < \pi/2$ ($R_{St}/H > 0.9$), the total fraction of ionizing photons that escape is

$$f = \tfrac{1}{2} (1 - \tfrac{3}{2} \sin \theta_c + \tfrac{1}{2} \sin^3 \theta_c) \, . \tag{14}$$

Equation (14) yields limiting values $f = 0$ when $\theta_c = \pi/2$ (no escape of ionizing photons) and $f = \frac{1}{2}$ when $\theta_c = 0$ (the escape of all upward traveling photons).

In § 2 the scale height near the W4 region was estimated to be $H \simeq 25$ pc, so that the critical value is $R_{St} = 22.5$ pc. For the W4 superbubble $\Phi_* = 2.3 \times 10^{50}$ s^{-1}, so that the critical density is $n_0 = 40$ cm^{-3}. Therefore it appears likely that during the *initial* illumination of the stratified ambient ISM, before any expansion via winds, extensive ionization would have occurred, with ionizing photons escaping to heights far above the cluster. In fact, we estimate $n_0 \simeq 10$ cm^{-3} below, which gives $R_{St}/H \simeq 2.3$, $\theta_c \simeq 23°$, and $f \simeq 0.22$. We emphasize that this is just the initial stage. Later, when the material is swept into a shell by the wind, the escape fraction f can change (see § 3.2.1).

3.2. *The Illumination of Wind-swept Cavities*

Given the remarkable similarity in appearance between the W4 superbubble and the wind-blown bubble model presented in the last section, we consider the illumination of such a cavity by the ionizing photon flux from a central OB association.

3.2.1. *Structure of the Ionization Front*

As discussed in § 2.1, the superbubble is filled with a tenuous hot medium; this does not provide significant attenuation of the ultraviolet radiation field. The swept-up gas from the bubble is deposited along the cavity walls and is ionized by the Lyman continuum photon flux from the central OB association. The pressure within the superbubble is determined from the time-dependent Kompaneets solution (§ A.2). Since the pressure within the cavity is much larger than the pressure in the ambient stratified medium (even when photoheated to 10^4 K), the swept-up material, which is in approximate pressure equilibrium with the interior of the superbubble, is squeezed to higher density than the ambient material. The density within the ionized zone of the swept-up shell is calculated below. Owing to the n^2 dependence of the recombination rate, an important property of a wind-blown shell is that it absorbs a greater number of ionizing photons than the equivalent amount of matter in the undisturbed medium. The fraction of the shell that is ionized is easily determined by balancing ionizing photons and recombinations along a path from the central OB association through the shell.

The ionization front is located where the Lyman continuum photon flux becomes negligible. We compute this as a function of elevation angle θ. For each θ three possible ionization states exist: (1) The ionization front may occur within the high-pressured swept-up shell, in which case a very dense but cold neutral hydrogen (possibly molecular) outer shell surrounds the ionized material. (2) The Lyman continuum flux may escape the swept-up shell, only to produce an ionization front further out in the undisturbed stratified ISM. (3) The entire column along θ may be ionized, releasing Lyman continuum photons far beyond the bubble. State 2 is fairly rare in our model, because the swept-up material is very dense compared with the ambient exponentially stratified ISM, so that if Lyman continuum photons penetrate through the shell, they will likely break out of the atmosphere.

To quantify the above discussion, consider a segment of the shell located at an angle θ and distance s with respect to the central OB association. The shape of the bubble is completely specified in terms of the dimensionless parameter $\tilde{y}$. The surface density $N(\theta, y)$ within this shell segment can be computed as described in § 2.2.2 and is proportional to $n_0 H$. We take the pressure within the shell to be $P_s(y) = 2P(y)$, where $P(y)$ is the average pressure in the bubble computed from the Kompaneets solution. This is a reasonable estimate when using a thin-shell approximation (see Bisnovatyi-Kogan & Silich 1995, their § II.c). The number density of hydrogen nuclei in the shell is therefore

$$n_{II} = \frac{P_s(y)}{2 \, k \, T_{II}} \, . \tag{15}$$

Dimensional values for n_{II} can be obtained using the dimensional pressure in the shell $P_s = 2\tilde{P} \, (\rho_0 \, L_0^2/H^4)^{1/3}$, where $\tilde{P}$ has a lower bound $\simeq 0.02$ at late times (see discussion in § A.2). For example, using $T_{II} = 8000$ K and $n_0 = 10$ cm^{-3} (estimated below), we find that $n_{II} = 14.5$ cm^{-3} at late times. The maximum thickness of the ionized shell perpendicular to the local tangent is

$$\Delta R = N(\theta, y)/n_{II} \, . \tag{16}$$

For an ionizing flux Φ_*, the shell is ionized along the line-of-sight from cluster center to a depth approximated by

$$\Delta s \simeq \left(\frac{\Phi_*}{4\pi n_{II}^2 \, \alpha_B \, s^2} \right) . \tag{17}$$

The ionization depth perpendicular to the shell tangent,

Δs_R, requires multiplication of equation (17) by $\cos\phi$, where ϕ is the angle between the line-of-sight direction and the surface normal, yielding

$$\frac{\Delta s_R}{\Delta R} \simeq \left(\frac{\Phi_* \cos\phi\, kT_{\rm II}}{2\pi N_s P_s \alpha_B s^2}\right). \quad (18)$$

If $\Delta s_R > \Delta R$, the entire shell is ionized, and the Lyman continuum photon flux illuminates the ambient stratified ISM outside the bubble. If $\Delta s_R < \Delta R$, the ionization front occurs within the shell, and a much denser, cold shell layer in approximate pressure equilibrium overlies the ionized layer. Note that raising the ionizing flux, lowering the surface density, and lowering the pressure inside the bubble enhance the ability of Lyman continuum photons to penetrate through the shell. Determination of the location of the ionization front, if it exists outside the shell, is a straightforward adaptation of the method described in § 3.1.

The location of the ionization front determines the appearance of the superbubble in the H I observations. If the ionization front is always confined within the swept-up shell, then the region should appear as a closed bubble in the H I channel maps. However, if the Lyman continuum photons escape the shell along lines-of-sight above a critical θ, then the ambient medium within a cone of angle $\pi/2 - \theta$ around $\hat{z}$ will be entirely ionized, and the region will appear as a "chimney" in the H I channel maps. Hα observations complement the H I channel maps by highlighting the dense ionized gas within the shell even if the ionizing photons have penetrated into the low-density medium beyond it. Thus the different morphologies for the W4 superbubble described in NTD (H I: chimney) and DTS (Hα: closed bubble) are reconciled if the Lyman continuum flux breaks out toward the pole.

The height at which breakout of the Lyman continuum photons from the dense shell can occur depends on the amount of material that has been swept up and on the pressure in the bubble, which sets the density within the ionized component of the shell. In § 2.2.2, the surface density of the shell was shown to vary dramatically from the base of the bubble to the top, decreasing faster than the increase in surface area (which varies as s^2) because of curved streamlines. Thus breakout is expected to occur first at the top. Although such quantities as the pressure and age of the bubble and the surface density of the shell can be calculated in dimensionless form, where the units are the appropriate combination of n_0, L_0, and H, no dimensionless model exists when a fourth parameter Φ_* is included. Therefore specific dimensional models must be computed and analyzed. However, all the relevant variables except the number density are reasonably determined for the W4 superbubble, requiring only a one-dimensional search. The opening angle of the chimney observed in the H I channel maps is the basis for determination of n_0. Figure 6 shows the location of the ionization front compared with the inner edge of the cavity for various values of n_0. First we estimate analytically the value of n_0 at which the ionization front becomes trapped in the shell near $z = 0$. The trapping condition, $\Delta s_R < \Delta R$, can be rewritten using equation (18) as

$$N > \frac{\Phi_* kT_{\rm II}}{4\pi s^2 \alpha_B P}, \quad (19)$$

where $P = \frac{1}{2}P_s$ and $\cos\phi \simeq 1$. Furthermore, on dimensional grounds one expects that

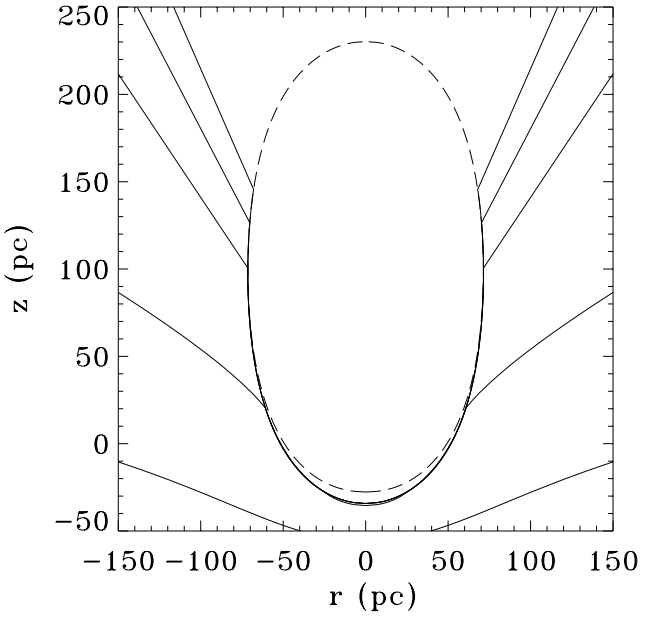

FIG. 6.—Location of the ionization front around a wind-swept bubble assuming the Kompaneets solution ($\tilde{y} = 1.98$), the stellar properties outlined in the text and varying only n_0, and the number density in the ionized exponential atmosphere ($H = 25$ pc) at $z = 0$. From bottom to top, $n_0 = 1$, 5, 10, 15, and 20 cm^{-3}. The dashed line plots the inner boundary of the ionized wind-swept shell.

$$N = \tilde{N} n_0 H, \quad (20)$$

$$s = \tilde{s} H, \quad (21)$$

$$P = \tilde{P}(\rho_0 L_0^2/H^4)^{1/3}. \quad (22)$$

The Kompaneets solution gives values for the dimensionless constants $\tilde{N}$, $\tilde{s}$, and $\tilde{P}$ at the current epoch, namely, $\tilde{N} \simeq 0.7$ at $z = 0$, $\tilde{s} \simeq 2$ at $z = 0$, and $\tilde{P} \simeq 0.02$. Using these relations, equation (19) is transformed into the condition

$$\begin{aligned} n_0 &> \left(\frac{1}{\tilde{N}\tilde{P}\tilde{s}^2}\right)^{3/4}\left(\frac{\Phi_* kT}{4\pi\alpha_B}\right)^{3/4}\left(\frac{1}{\mu m_{\rm H} L_0^2 H^5}\right)^{1/4} \\ &= 4.7\left(\frac{0.02}{\tilde{P}}\right)^{3/4}\left(\frac{0.7}{\tilde{N}}\right)^{3/4}\left(\frac{2}{\tilde{s}}\right)^{3/2}\left(\frac{\Phi_*}{2.3\times10^{50}\ {\rm s}^{-1}}\right)^{3/4} \\ &\quad \times \left(\frac{T}{8000\ {\rm K}}\right)^{3/4}\left(\frac{3\times10^{37}\ {\rm ergs\ s}^{-1}}{L_0}\right)^{1/2} \\ &\quad \times \left(\frac{25\ {\rm pc}}{H}\right)^{5/4}\ {\rm cm}^{-3}. \end{aligned} \quad (23)$$

Figure 6, which is obtained using the same normalizing values as in equation (23), also shows that the ionization front is trapped within the shell at $z = 0$ when $n = 5$ cm^{-3}. As n_0 is increased further, the ionization front gets trapped to progressively greater heights. For fixed n_0, the ionization front opens outward in a conelike fashion above a critical height, since neither the shell nor the low-density medium beyond it are able to confine the ionizing photons. Beyond a density $n_0 \simeq 10$ cm^{-3}, this opening point of the ionization front rises very slowly with increasing n_0, since most of the original mass is deposited within a few scale heights of the cluster (see the streamlines in Fig. 1). We find our best-fit model to the W4 superbubble by picking the model whose

ionization front turnoff point coincides with the height of significant drop off of H I emission. For NTD, this occurs at about 2°.9 ($\gtrsim$100 pc) above the cluster (see Fig. 2). This opening point is bracketed by the $n_0 = 10$ cm^{-3} and $n_0 = 15$ cm^{-3} curves, with $n_0 \simeq 10$ cm^{-3} a reasonable best fit. Further H I observations should be able to confirm whether the apparent drop-off in H I emission continues at higher latitudes, which would be consistent with the idea that the ionizing photons have penetrated the shell at heights $\gtrsim$100 pc. It is interesting to note that the density estimate $n_0 \simeq 5$ cm^{-3} made by NTD by looking at H I gas adjacent to the chimney and at the latitude of the cluster is about the same as the minimum density allowed by our model (eq. [23]). Furthermore, it is in good agreement with our derived most likely value $n_0 \simeq 10$ cm^{-3}, given the uncertainties in both the observations and in some of our model parameters.

The fraction of Lyman continuum photons that escape the superbubble can be determined from these models and the analytic formulae described in § 3.1. For low-density environments, little material is swept up by the expanding bubble, and although the bubble appears brighter than the background, the fraction of ultraviolet photons trapped by the shell is insignificant; the escaping fraction may be deduced from the arguments for a static exponential atmosphere, i.e., equations (13) and (14). However, when the density of the medium is large enough, the exponential atmosphere becomes insignificant for this calculation, and the fraction of photons that escape is determined by the absorption within the illuminated shell. For our best-fit model ($n_0 \simeq 10$ cm^{-3}), the fraction of solid angle through which ionizing photons escape (when $\tilde{y} = 1.98$) is approximately 15%. At these opening angles, the shell is at a relatively high latitude and contains little mass, so that nearly all the ionizing flux is transmitted. Therefore we calculate that a flux of ionizing photons $\simeq 0.15\ \Phi_* \simeq 3 \times 10^{49}$ s^{-1} from the cluster OCl 352 escapes to higher latitudes.

Below $z \simeq 100$ pc, and particularly in the downward direction ($z < 0$), this model predicts that the stellar cluster does not completely ionize the dense wind-swept shell. There should then be a cooler, even more dense shell outside the ionization front, again in approximate pressure equilibrium. It is therefore interesting that the *IRAS* observations show peak emission just outside the ionized shell along the lower part of the cavity (Heyer & Terebey 1998). For maximum conversion of stellar into reradiated infrared luminosity by dust, the shell should have substantial optical depth. This can be checked by noting that the column density at $z \simeq z_2$ is $\sim n_0 H \simeq 10^{21}$ cm^{-2} (see Fig. 4) for our standard values of n_0 ($\simeq 10$ cm^{-3}) and H ($\simeq 25$ pc). For a normal dust to gas ratio, this implies that $A_V \sim 0.5$ mag, yielding significant self-obscuration of our view into the lower bubble. Accompanying this optical depth, we have the possibility of molecular gas (which might be swept up, having survived the earlier evolution, or have reformed). Heyer & Terebey (1998) also show CO emission confined along a thin layer adjacent to the bottom edge of the superbubble, indicating the presence of dense swept-up molecular gas.

3.2.2. *Emission Measure*

Considering the evolutionary scenario for a wind-blown superbubble outlined in § 3.2.1, it is straightforward to produce models of the emission measure profile, $\int n^2\, dl$, where the integral is taken through the bubble along our line-of-sight, for a variety of n_0 values (Figs. 7*a*–7*c*). In each panel, six epochs are shown corresponding to $\tilde{y} = 0.5$–1.98, and the emission measure is presented as a gray scale, with darker regions corresponding to higher emission measure. A cavity in H I channel maps should occur wherever emission is observed; in these regions the gas is ionized. Each figure also shows the instantaneous location of the ionization front separating the ionized from the neutral gas. Thus, when n_0 in the ambient ISM is low, as in Figure 7*a*, the region always appears as a giant cavity in H I . The ionization front occurs in the ambient medium outside the shell, so that in Hα or radio continuum the region shows a thin-shelled bubble with a very bright halo beneath. As n_0 is increased, the H I chimney narrows and the bright Hα halo disappears from beneath the bubble. In the highest density case presented ($n_0 = 10$ cm^{-3}), the upper shell is opaque to the ionizing photons for a time, once sufficient mass is swept up into it, but eventually becomes transparent when the internal pressure (and the density of the shell) has dropped sufficiently.

The Hα shell thickness observed by DTS falls in the range 0°.2–0°.5 at all heights. Our model predicts a thick shell near the bottom of the bubble and an extremely thin shell (much thinner than observed by DTS) in the upper portion of the bubble (Figs. 7*a*–7*c*). The former is due to the large amount of mass swept up in the increasing exponential atmosphere below $b = 0°.9$ ($z = 0$), which is probably not a good representation of the atmosphere there, and the latter is due to the uniform pressure assumed in the bubble (see § A.2 for further discussion). A much lower pressure should exist near the top of the bubble at this stage, allowing for a thicker shell there. However, our model should give a reasonable estimate for the shell thickness near $z = 0$. The maximum shell thickness there can be found by combining equations (15), (16), (20), and (22), yielding

$$\Delta R = \frac{\tilde{N}}{\tilde{P}} \frac{n_0^{2/3} H^{7/3} kT}{(\mu m_{\rm H})^{1/3} L_0^{2/3}}$$
$$= 11.1 \left(\frac{\tilde{N}}{0.7}\right)\left(\frac{0.02}{\tilde{P}}\right)\left(\frac{n_0}{10\ {\rm cm}^{-3}}\right)^{2/3}$$
$$\times \left(\frac{H}{25\ {\rm pc}}\right)^{7/3}\left(\frac{3 \times 10^{37}\ {\rm ergs\ s}^{-1}}{L_0}\right)^{2/3} {\rm pc}\ . \quad (24)$$

At a distance $d \simeq 2.35$ kpc, the standard value obtained above yields

$$\Delta\theta = \frac{\Delta R}{d} \simeq 0°.27\ , \quad (25)$$

which falls within the range observed by DTS.

A direct comparison between the Hα emission produced by the best-fit model of the ionized wind-swept bubble ($n_0 = 10$ cm^{-3}; last frame of Fig. 7*c*) and the Hα observation of DTS reveals the merits of the simulation. Conversion between emission measure and Rayleigh flux units (R) is straightforward: at $T_{\rm II} = 8000$ K, 1 R = 2 pc cm^{-6}. DTS compute an extinction at Hα of 2.1 mag toward the star cluster, which we apply as a uniform obscuring medium to the model bubble. Also, as shown in Figure 8, the intensity profile of the DTS observation (averaged over 9 pixels or 9 pc) along the symmetry axis $r = 0$ reveals a high background flux below the bubble and a low background flux above the bubble (*thin line*). We empirically model this

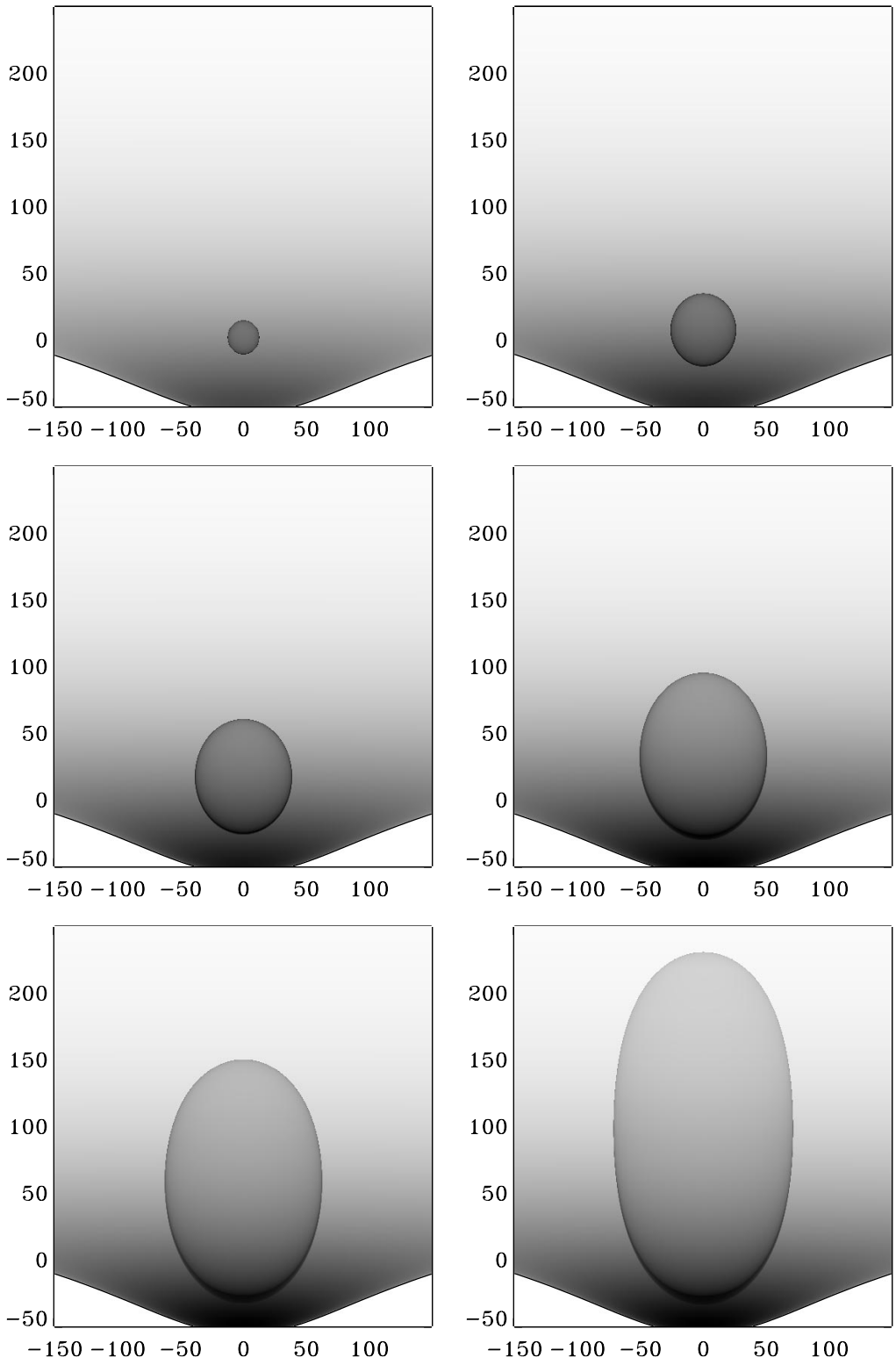

FIG. 7*a*

FIG. 7.—Relative emission measure across an expanding bubble ionized by an internal cluster of stars with properties outlined in the text. Within an exponential atmosphere ($H = 25$ pc), six stages in evolution are represented ($\tilde{y} = 0.5$, 1.0, 1.4, 1.7, 1.9, and 1.98). Distances are labeled in pc on both axes, with the star cluster located at (0, 0): (*a*) $n_0 = 1$ cm^{-3}. Note that the ionization front is always well separated from the bubble. (*b*) $n_0 = 5$ cm^{-3}. In this case the increasing column density at the base of the bubble confines the ionization front at late stages. (*c*) $n_0 = 10$ cm^{-3}, representing the best case scenario for the W4 superbubble. Note that the ionization front is initially open toward the top, is confined by the high-density swept-up shell at intermediate epochs, and then breaks out when the bubble gets elongated.

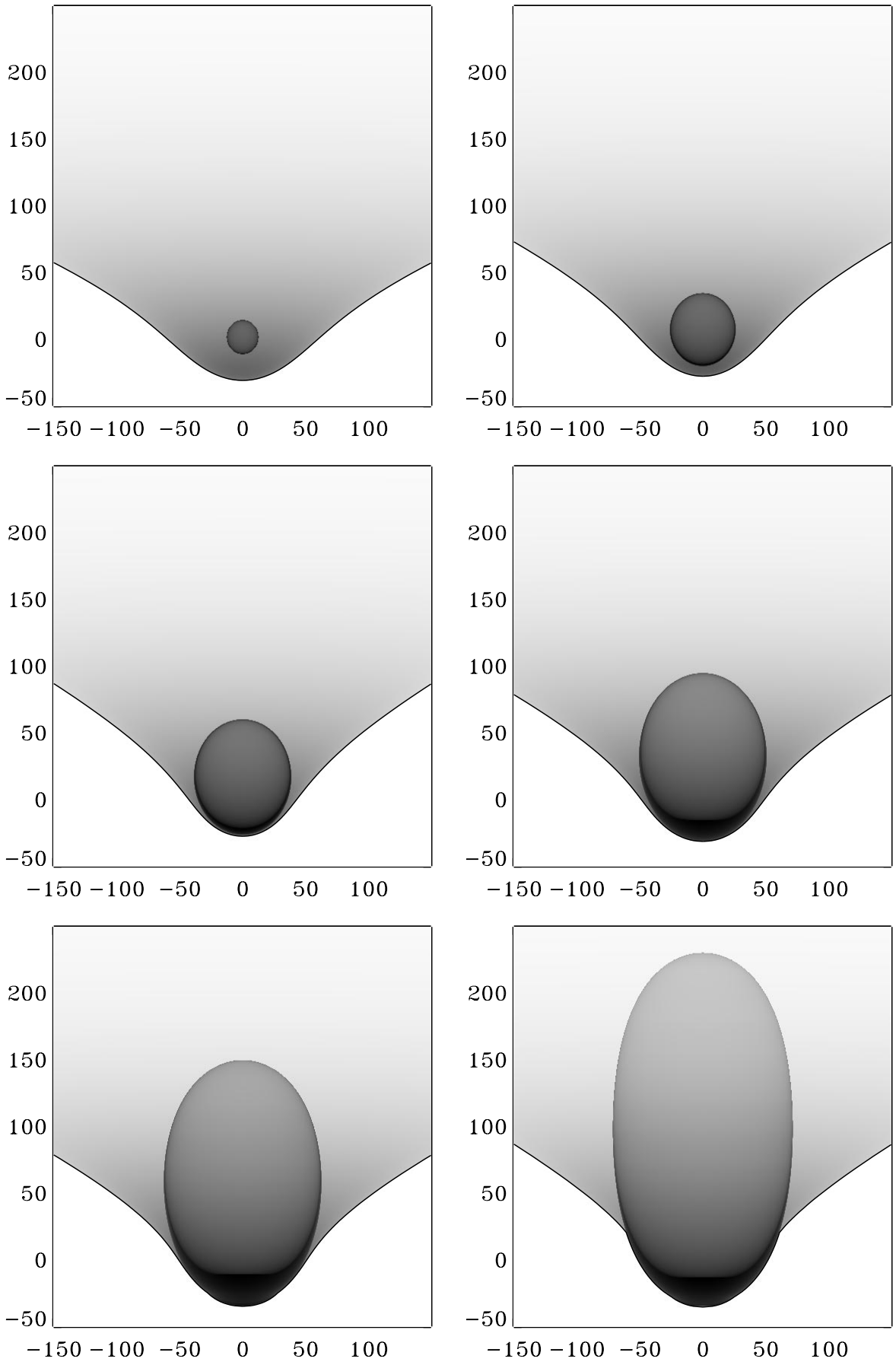

FIG. 7*b*

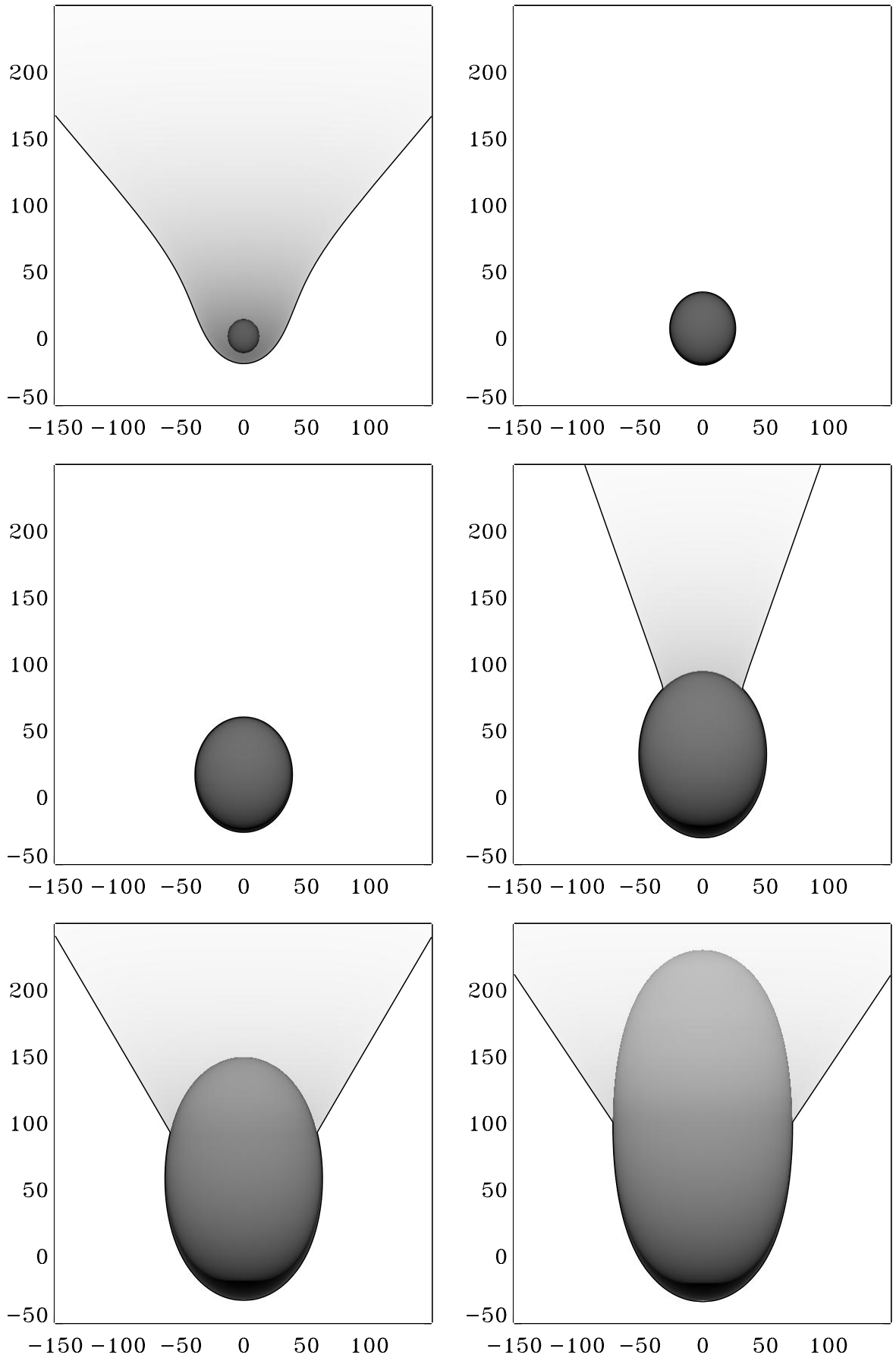

FIG. 7*c*

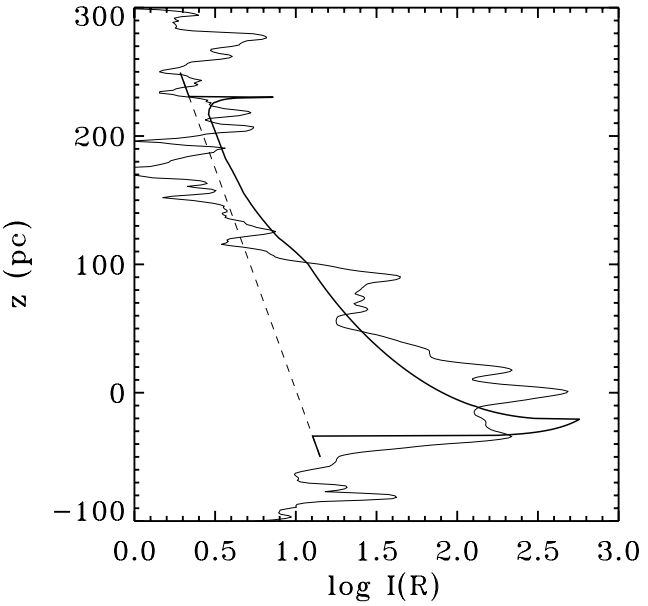

FIG. 8.—Hα intensity profile along the symmetry axis ($r = 0$) of the superbubble. The thick line represents the model described in Fig. 7*c* after conversion to Rayleighs with addition of background flux (*dashed line*), as described in text, and extinction by 2.1 mag. The thin line represents the intensity profile observed by DTS along a vertical cut centered on the cluster OCl 352.

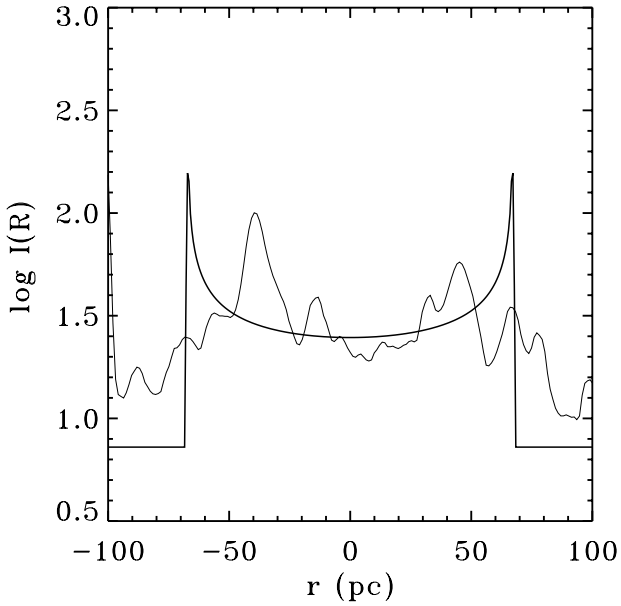

FIG. 9.—Hα intensity profile across the model superbubble at a height $z = 50$ pc above the cluster. The thick line represents the model described in Fig. 7*c* after conversion to Rayleighs, the addition of background flux (see text), and extinction by 2.1 mag. The thin line represents that observed by DTS.

background as an exponential distribution with a characteristic scale of 3°.3 and a 140 R normalization at $b = 0°.9$ (the latitude of the stellar cluster) before attenuation (Fig. 8, *dashed line*). The best-fit model including the empirical background and attenuation to the bubble is also shown in Figure 8 (*thick line*). The overall profiles match remarkably well despite the many internal knots of emission appearing in the observations that have not been modeled. The brightness of the model at the bottom of the shell ($z \lesssim -20$ pc) is significantly greater than the observed Hα flux. This deficit of observed Hα flux was also noted by DTS and arises in comparison with any model that assumes that the bottom of the shell is ionization bounded, since the Hα brightness is then determined by the ionizing flux. A possible explanation for the discrepancy is extinction due to dense swept-up neutral gas outside the ionization front ($A_V \sim 0.5$ mag; see earlier discussion). However, the edge-brightening enhancement at the bottom shell appears reasonable, as does the slow decline in brightness with height. The intensity declines in two stages, separated at $z \simeq 100$ pc, which marks the position within the model where the ionization front breaks through the wind-swept shell. Both components appear visible in the Hα observations.

In Figure 9, an intensity profile is produced across the bubble at a height $z = 50$ pc. The model has been attenuated in the same manner as discussed for Figure 8 (at this height the background flux is 100 R in the empirical model). The Hα data reveals enhanced emission within the bubble comparable to the level expected from the model, but the two wall features are not observed. An intensity peak of the correct magnitude is observed at $r = -40$ pc and is consistent with the fact that the Hα shell is pinched at low latitudes (Fig. 3). As noted above, the thickness of the observed peak is greater than derived in the model, indicating that at this latitude the pressure in the bubble may not be as high as expected from a simple Kompaneets solution. The bubble edge is not apparent on the right-hand side; however, the intensity does decrease significantly where the edge should be. Part of the difficulty in matching the edge-brightened intensities may be the requirement, satisfied in the model but perhaps not in reality, of significant coherence along our line-of-sight. If the thin bubble wall has nonaxisymmetric structure, then the intense edge emission will be spread over a larger area, and the bright cusp will not be observed.

4. DISCUSSION

Given the best-fit parameters $n_0 \simeq 10$ cm^{-3}, $L_0 \simeq 3 \times 10^{37}$ ergs s^{-1}, and $H \simeq 25$ pc for the W4 superbubble, equation (9) yields the best-fit age estimate,

$$t \simeq 2.5 \text{ Myr} . \tag{26}$$

This is less than the estimated main-sequence lifetime (3.7–4.3 Myr) of the O stars in the cluster (NTD) and is therefore consistent with NTD's interpretation that the superbubble is blown by the combined winds of the young cluster in which no supernovae have yet occurred. The cluster age has also been estimated by various authors to be ≤ 2.5 Myr (see DTS). The superbubble is on its way to blowing out of the Galactic disk unless the atmospheric structure changes significantly at greater heights. Given our best-fit parameters, the blowout parameter (defined in § 2.1) $b \simeq 25$ (see eq. [6]), so that use of the Kompaneets model is justified. A quick estimate of the superbubble age can also be made using an important feature of expansion in a stratified atmosphere pointed out in § A.2; the base radius at $z = 0$, about 50 pc in this case, can be equated to R_s in the spherical solution (eq. [1]), and our best estimates for n_0 and L_0 used to obtain $t \simeq 2.1$ Myr. This is in reasonable agreement with the value (eq. [26]) determined directly from the Kompaneets model.

The shape of the W4 superbubble provides an important surprise: the ambient interstellar gas around the cluster

OCl 352 was very strongly stratified in the vertical direction. The estimated scale height $H \simeq 25$ pc is based on the best-fit Kompaneets profile and the estimated distance 2.35 kpc to the cluster. This is to be compared with typical estimates $H \gtrsim 100$ pc for interstellar gas near the Galactic plane based on emission from H I or CO. For example, the FCRAO CO survey of the outer Galaxy (Heyer et al. 1998), where the Perseus arm lies, finds an overall mean CO scale height of 113 pc.[1] Our scale height determination is, in contrast, based on a dynamical model of an observed superbubble and is applicable only to the immediate vicinity of the stellar cluster OCl 352 and the W4 H II region. Our scale height estimate would increase linearly in proportion to the cluster distance if it were actually farther than the 2.35 kpc recently determined by the spectroscopic parallax method (Massey et al. 1995). However, we do not expect the actual distance to be much different, since many previous estimates for the distance to OCl 352 or the W3/W4/W5 H II regions have, using a variety of techniques, yielded values in the range 1.6–2.7 kpc (see NTD). Similarly, the estimate $H \simeq 25$ pc cannot be explained away as a result of any of the simplifications of the Kompaneets model. All models for bubble expansion, whether analytic, semi-analytic, or numerical (e.g., Kompaneets 1960; MacLow & McCray 1988; Tomisaka & Ikeuchi 1986; MacLow et al. 1989), show that the bubble remains nearly spherical as long as the ratio of the radius in the plane $z = 0$ to the scale height $R/H < 1$. Significant elongation takes place only when $R/H \gtrsim 2$, i.e., the bubble has had a chance to fully sample the stratified atmosphere. The W4 superbubble is currently highly elongated and has a radius in the plane $R \simeq 50$ pc, hence one can conclude that $H < 50$ pc, and most likely $H \approx 25$ pc, using very simple physical arguments.

The relatively small value of H in comparison to the mean ISM value ($\gtrsim 100$ pc) implies that significant vertical compression of the interstellar gas has taken place here, perhaps not such a surprising finding for a star-forming region. Consistent with this, the most likely value for n_0 ($\simeq 10$ cm^{-3}) is also significantly greater than the mean ISM value (~ 1 cm^{-3}). It is interesting to note that the total surface density of gas, which is proportional to $n_0 H$, is about a factor of 2 greater than implied by the mean ISM values. This is consistent with the idea that some lateral inflow of gas has also taken place during the assembling of the molecular cloud.

The Kompaneets model idealizes the atmosphere as being purely exponential, so it is all the more striking that the $\tilde{y} = 1.98$ profile provides such a good approximation to the overall shape of the superbubble (Fig. 3). Thus the exponential atmosphere and scale height $H \simeq 25$ pc should be reasonable approximations for the mean atmosphere into which the superbubble has expanded. At large heights, toward the top of the superbubble, it is possible that the stratification is not so great. Although there is relatively little mass there, it may be more than implied by an exponential atmosphere with $H \simeq 25$ pc. Possible deviations from the assumed atmosphere, e.g., the extent to which the medium with $H \simeq 25$ pc can be embedded in one with larger H at high latitudes and/or adjacent longitudes, can be best addressed with future modeling using the thin shell approximation or numerical models. However, we note that various models of bubble expansion (e.g., MacLow & McCray 1988) have shown that a bubble changes shape dramatically when it travels from a relatively low scale height atmosphere (e.g., the H I cloud layer) to one with greater scale height (e.g., the H I intercloud layer); that is, the bubble radius expands to become comparable to the local scale height. This sort of expansion has not yet happened to the W4 superbubble. Hence we conclude that the effect of extra mass near the top of the bubble cannot be very great.

Below the star cluster, the density probably decreases eventually, certainly on passage past the midplane of the Galaxy, unlike the increasing exponential function in the Kompaneets model. However, the presence of a decreasing density gradient in the downward direction must be much less pronounced than that above the cluster, or else the superbubble would blow out in both directions. The finite pressure of the external medium may also play a role in confining the downward expansion.

Deviations from a pure exponential atmosphere are already evident in Figures 2 and 3. Figure 3 reveals that the superbubble is narrowest at a latitude almost equal to that of the star cluster. Such a pinch is usually caused by a local maximum in the density (e.g., MacLow & McCray 1988). There is clear evidence for high-density regions that inhibit the expansion immediately adjacent to the cluster; CO and *IRAS* images reveal a dense cloud near the left (east) pinch, and the right-hand (west) side is certainly affected by the presence of the W3 molecular cloud.

Further evidence for a more complicated atmosphere is provided by the H I and CO maps (NTD; Heyer et al. 1996), which reveal embedded clouds in the cavity. These clouds are most likely remnants of an initially clumpy medium; a superbubble can move around dense clumps and continue to expand (MacLow & McCray 1988). The CO maps reveal two cometary shaped clouds (Heyer et al. 1996), and NTD find a V-shaped filament in H I (visible in Fig. 2) with the higher latitude CO cloud at its base. The V-shaped "streamers" are suggestive of material being stripped from the molecular cloud by a free-streaming wind, but Heyer et al. (1996) argue that the cometary shape of the CO clouds is likely due to the sculpting effects of the ionizing UV radiation field of the O stars. Our model supports the view that the CO clouds are embedded in a hot rarefied gas in which the ionizing UV radiation from the central source propagates freely, i.e., region 2 in the description of a wind-blown bubble given in § 2.1. Region 1, consisting of free-streaming wind, remains relatively small during the evolution because of the high pressure in the hot shocked region 2. We estimate the current radius of this region to be $R_1 \simeq 10$ pc (see Appendix B). For comparison, the bottom of the lower latitude embedded CO cloud observed by Heyer et al. (1996) is about 16.5 pc above the cluster. We note that photoevaporation of these clouds will act to cool the shocked gas in the bubble interior (McKee, Van Buren, & Lazareff 1984) and slow down the expansion of the bubble. This will tend to increase the inferred age of the bubble given by equations (9) and (26).

[1] One should note that this is based on kinematic distances determined by the standard circular rotation curve of the Galaxy, which can overestimate the distance for gas in a spiral arm, thereby also overestimating the scale height. Heyer & Terebey (1998) point out this effect; the kinematic distance to OCl 352, based on associated molecular gas, ranges from 3.5 to 4.0 kpc, while the spectroscopic distance to OCl 352 is only 2.35 kpc (Massey et al. 1995).

The thickness of the ionized shell in our model agrees well with observations of the superbubble near $z = 0$, as shown in § 3.2.2. However, the shell thickness in our model becomes progressively thinner at high latitudes than revealed by the Hα map of DTS. This can be due to several reasons. As explained in § A.2, our estimate of the pressure applies only near the base of the bubble. In reality, a pressure gradient must be present in the bubble at this stage, so that the pressure is much lower near the top, allowing for a thicker (but less bright) shell there. Additionally, a swept-up magnetic field may contribute significant pressure within the shell and prevent it from being compressed to the level in our model. A tangential magnetic field within the shell might also explain another puzzling feature of the observed superbubble. The Kompaneets model and indeed all expansion models predict that a bubble is in the rapidly accelerating blowout phase by the time it is so elongated (recall the decelerating expansion only lasts while the bubble is within one or two scale heights above the source and still has a nearly spherical shape). Hydrodynamic simulations of expanding superbubbles show that the shell fragments during this stage due to a Rayleigh-Taylor instability (MacLow et al. 1989). Yet the Hα map of DTS shows that the W4 supershell is relatively smooth. A plausible explanation for the suppression of the Rayleigh-Taylor instability is the stabilizing effect of a swept-up tangential magnetic field in the shell (e.g., the simulations of Stone & Norman 1992). We investigate this issue further in a future paper; preliminary results can be found in Komljenovic, Basu, & Johnstone (1999).

While magnetic fields might explain some features of the W4 superbubble, we caution that they can also raise complications. For example, a dynamically significant magnetic field aligned predominantly parallel to the Galactic plane would prevent the bubble from attaining its present elongated shape, both by potentially increasing the scale height H and also by exerting a force that inhibits expansion perpendicular to the plane. Indeed, simulations of bubble expansion in a stratified medium with a dynamically significant field parallel to the Galactic plane show that the bubble expands preferentially *along* the Galactic plane (Tomisaka 1992), unlike the W4 superbubble.

Our model for the ionization structure of the bubble also predicts that a significant fraction ($\simeq 15\%$) of the ionizing UV photons from the cluster escape above the bubble. Although the top of the W4 superbubble is at a height $z_1 \simeq 246$ pc and we have no information about the density structure above the superbubble, it is quite likely that if the ionizing photons can penetrate the dense upper shell of the bubble they will then continue to ionize the higher regions of lower density. The escape of ionizing photons is ultimately traced to the relatively low scale height H of the local medium in comparison to the initial Strömgren sphere radius of the combined O stars. If relatively low values of H, on the order of the value found in this paper, are common around major star-forming regions and young star clusters, then the consequent penetration of ionizing UV photons far above the Galactic plane may be a natural explanation for the extensive presence and large scale height (>1 kpc) of free electrons in our Galaxy (e.g., Reynolds 1989, 1991).

5. SUMMARY

We have used a model for the dynamical expansion and ionization structure of a superbubble to gain insight into ISM conditions near the young cluster OCl 352. The Kompaneets solution provides a reasonable fit to the observed shape of the H I cavity and Hα shell of the W4 superbubble, and when combined with a distance to the cluster, yields an estimate for the mean scale height H of the local atmosphere. Remarkably, we find that $H \simeq 25$ pc in this star-forming region, significantly less than the mean ISM value near the Galactic plane. This relatively low value is an unavoidable conclusion given the significant elongation of the superbubble. The Kompaneets solution also allows us to estimate the current pressure near the base of the superbubble. This estimate, along with properties of the ionized shell of the superbubble, enable us to constrain the value of the original ambient density n_0 near the cluster. The total wind luminosity of the massive stars L_0 can be estimated from observations and/or the spectral type of the stars (Normandeau et al. 1996). Therefore we can use the best values for n_0 ($\simeq 10$ cm^{-3}), L_0 ($\simeq 3 \times 10^{37}$ ergs s^{-1}), and H ($\simeq 25$ pc) to find a dimensional value for the age of the superbubble. Our estimated age of 2.5 Myr is consistent with the age of the cluster and the idea that the superbubble is blown by the combined winds of the cluster stars, among which no supernovae have yet occurred.

We have calculated the ionization structure of a stratified medium, both before and during the expansion of a superbubble within it. The combined photoionizing ability of the nine O-type stars is sufficiently high and the ambient scale height H of the medium sufficiently low that initially the ionizing photons escape to heights far above the cluster. The expansion of the superbubble creates a dense shell, which could even trap all the ionizing photons for a time. However, during the late stages, when the bubble pressure (and therefore the shell density) has dropped sufficiently, the ionizing photons penetrate beyond the upper portions of the shell (of lower mass surface density) and escape to greater heights; the shell still traps the ionizing photons near the base ($z \lesssim 0$). This means that, while the upper shell will be an enhanced region of Hα emission, the superbubble will have no visible lid in H I. Thus, while the apparent closure of the Hα shell (Dennison et al. 1997) places a damper on the Galactic chimney hypothesis (at least at the present epoch), the W4 superbubble may continue to appear as a chimney when observed in H I at higher latitudes than in the CGPS Pilot project (Normandeau et al. 1996). Finally, if the presence of a relatively low scale height of gas is common near an OB cluster, the consequent escape of ionizing photons may provide a natural explanation for the extensive presence of ionized gas in our Galaxy.

We thank Brian Dennison for making his Hα data available to us. This work was supported by the Natural Sciences and Engineering Research Council (NSERC) of Canada. D. J. was supported by an NSERC Postdoctoral Fellowship. S. B. was partially supported by the CGPS/CSP grant from NSERC.

APPENDIX A

KOMPANEETS MODEL

A1. SPATIAL SOLUTION

The Kompaneets model assumes that the energy source is located at $z = 0$ in an exponential atmosphere (here the ISM) with density

$$\rho(z) = \rho_0 \exp(-z/H), \tag{A1}$$

where H is the scale height. Note that $z = 0$ is not necessarily the Galactic midplane. The model assumes that the internal pressure of the bubble dominates any external pressure: the atmosphere is pressure-free. This means that all bubbles will continue to expand in the z-direction; furthermore, the top of the shell will reach infinite z in a finite time, i.e., undergo blowout. Physically, we can use the Kompaneets model when we are confident that the external pressure P_e will not confine the bubble before the upper shell begins to accelerate; i.e., the parameter b (eq. [6]) must be significantly greater than one. This condition is certainly satisfied by the W4 superbubble, as shown in § 2.1.

The internal pressure of the bubble is taken to be constant, and it is

$$P = (\gamma - 1)\frac{E_{\rm th}}{\Omega}, \tag{A2}$$

where γ is the ratio of specific heats, $E_{\rm th}$ is the thermal energy of the bubble, and the volume Ω of the remnant is defined in cylindrical symmetric coordinates (r, z) by the integral

$$\Omega = \pi \int_{z_2}^{z_1} r^2(z, t)\, dz, \tag{A3}$$

in which z_1 and $z_2 (< 0)$ are the top and bottom of the remnant, respectively. The extremely high temperature of the shocked gas, and hence short sound crossing time, is the reason that the internal pressure is assumed to have readjusted to an isobaric state at all times. Since the internal pressure dominates the external pressure, the expansion speed is that given by the Hugoniot conditions for a strong shock,

$$v_n = \sqrt{\frac{\gamma + 1}{2}\frac{P(t)}{\rho(z)}}. \tag{A4}$$

The expansion is assumed to be directed normal to the local surface of the remnant. In the Kompaneets approximation, the mass swept up by the outer shock is assumed to reside in a thin shell behind the front, although the effect of its inertia is not included in the model.

Using equation (A4) and the assumption that the shock front moves normal to itself everywhere, Kompaneets (1960) derived an equation for the evolution of the shock front:

$$\left(\frac{\partial r}{\partial y}\right)^2 - \frac{\rho(z)}{\rho_0}\left[\left(\frac{\partial r}{\partial z}\right)^2 + 1\right] = 0 \tag{A5}$$

(see also Bisnovatyi-Kogan & Silich 1995). In equation (A5), y is a transformed variable (with units of length) defined by

$$y = \int_0^t \sqrt{\frac{\gamma^2 - 1}{2}\frac{E_{\rm th}}{\rho_0 \Omega}}\, dt. \tag{A6}$$

The thermal energy $E_{\rm th}$ of the bubble is calculated from the differential equation

$$\frac{dE_{\rm th}}{dt} = L_0 - P\frac{d\Omega}{dt}. \tag{A7}$$

This equation differs from that used in the blast wave formulation of the problem, in which $E_{\rm th}$ is a constant fraction of the energy deposited in an initial blast. Equation (A7) assumes that the wind luminosity is thermalized at the inner shock front R_1 and that the only energy loss is due to work done against the thin shell. The effect of radiative and evaporative cooling of the bubble interior can also be added here if desired.

Kompaneets (1960) showed that equation (A5) could be solved analytically by separation of variables, yielding the relation

$$r(z, y) = 2H \arccos\left[\frac{1}{2}e^{z/2H}\left(1 - \frac{y^2}{4H^2} + e^{-z/H}\right)\right]. \tag{A8}$$

Equation (A8) describes a sequence of shapes for the shock front, which change as the parameter y varies from 0 to $2H$, at which time the top of the remnant formally reaches infinity. Note that one can discuss the structure of the shock front without

actually solving for the explicit time-dependence y versus t (§ A.2) from equations (A6) and (A7). The top and bottom of the remnant, where $r = 0$, are located at

$$z_{1,2} = -2H \ln\left(1 \mp \frac{y}{2H}\right). \tag{A9}$$

The maximum radius of the bubble, where $\partial r/\partial z = 0$, is

$$r_{\max} = 2H \arcsin\left(\frac{y}{2H}\right). \tag{A10}$$

The above equations show that, by the time of blowout ($y = 2H$), the bubble has radius in the plane $r(z = 0) = 2.09H$ and a maximum radius $r_{\max} = \pi H$ and has penetrated downward into the atmosphere of exponentially increasing density to a location $z_2 = -1.39H$.

Equation (A8) illustrates an important property of the Kompaneets model: the spatial solution is independent of the time evolution. The shock front evolves through the sequence of shapes given by equation (A8), which is a consequence only of the atmospheric structure. However, the *rate* at which it evolves does depend on the details of the energy input into the bubble, i.e., whether the energy is input at one instant or in a continuous fashion and at what rate. Hence the shape of an observed bubble can supply information about the ambient atmosphere independent of any knowledge of the energetics of the driving source.

A2. TIME EVOLUTION

A numerical integration of equations (A6) and (A7) yields $y(t)$ and $E_{\rm th}(t)$, which implicitly give the time evolution of the bubble. The solution for a wind-blown bubble in an exponential atmosphere depends on only three parameters: the scale height H, the density near the source ρ_0, and the wind luminosity L_0. Hence the problem is solved most naturally in a system of units that are formed from these three parameters. The unit of length is then H, the unit of mass is $\rho_0 H^3$, and the unit of time is $(\rho_0 H^5/L_0)^{1/3}$. The units for various physical quantities under this system are listed in Table 1. We obtain the dimensionless solution by integrating the dimensionless form of equations (A6) and (A7). The dimensional solution for any combination of ρ_0, L_0, and H can be obtained from this single solution using the units shown in Table 1. In the following discussion, dimensionless variables are overlaid with a tilde sign. Figure 10*a* shows the parameter $\tilde{y}$ versus time $\tilde{t}$ in a solid line. The integration is carried up to $\tilde{y} = 1.98$, the stage at which the spatial profile matches the W4 superbubble. We do not integrate all the way to the limit $\tilde{y} = 2$ because of the artificial nature of the solution at that time; the top of the remnant reaches infinity at infinite speed, and the pressure drops to zero. For comparison, the dimensionless radius of the spherical expansion solution $\tilde{R}_s = 0.76\tilde{t}^{3/5}$ (from eq. [1]) is plotted alongside in a dashed line. The relationship between y and R_s helps to assign some physical meaning to y. For early times, when the expansion is nearly spherical, inserting the spherical homogeneous solutions for R_s (eq. [1]) and $E_{\rm th}$ (eq. [2]) into equation (A6) yields

$$\tilde{y} = 0.77\tilde{t}^{3/5} \tag{A11}$$

if we take $\gamma = \frac{5}{3}$. Therefore y is essentially equal to R_s at early times. However, Figure 10*a* also shows that $y \simeq R_s$ throughout most of the evolution. Although y begins to fall below R_s when the bubble has expanded beyond one scale height, it is only 14% below R_s when $\tilde{y} = 1.98$. Figure 10*b* shows the distance traveled by the bubble shell in three directions: (1) upward along the z-axis, i.e., $\tilde{z}_1$; (2) downward along the z-axis, i.e., $-\tilde{z}_2$; and (3) along the r-axis, i.e., $\tilde{r}(z = 0)$. The dimensionless spherical solution $\tilde{R}_s$ is again given for comparison in a dashed line. The top of the bubble z_1 eventually moves much farther than R_s, since it moves into a progressively lower density environment, whereas the bottom moves less far than R_s, because it moves into a progressively higher density environment. With constant density along $z = 0$, the time evolution of $r(z = 0)$ closely follows that of R_s, even though the curved streamlines mean that $r(z = 0)$ does not follow a mass element in a Lagrangian fashion. There is an even closer correspondence between y and $r(z = 0)$; even at the end of the integration, the two values differ by only 4%. Altogether, we find the important relation

$$y \simeq r(z = 0, y) \simeq R_s\,. \tag{A12}$$

Therefore the measurement of the radius $r(z = 0)$ of any observed bubble can yield quick estimates for y and even the age t (if one has estimates for L_0 and ρ_0), since R_s can be converted to a time through equation (1).

TABLE 1

UNITS OF PHYSICAL QUANTITIES

Physical Quantity	Unit
Length	H
Time.....	$(\rho_0 H^5/L_0)^{1/3}$
Velocity	$(L_0/\rho_0 H^2)^{1/3}$
Acceleration	$(L_0^2/\rho_0^2 H^7)^{1/3}$
Mass	$\rho_0 H^3$
Energy	$(\rho_0 L_0^2 H^5)^{1/3}$
Pressure.....	$(\rho_0 L_0^2/H^4)^{1/3}$

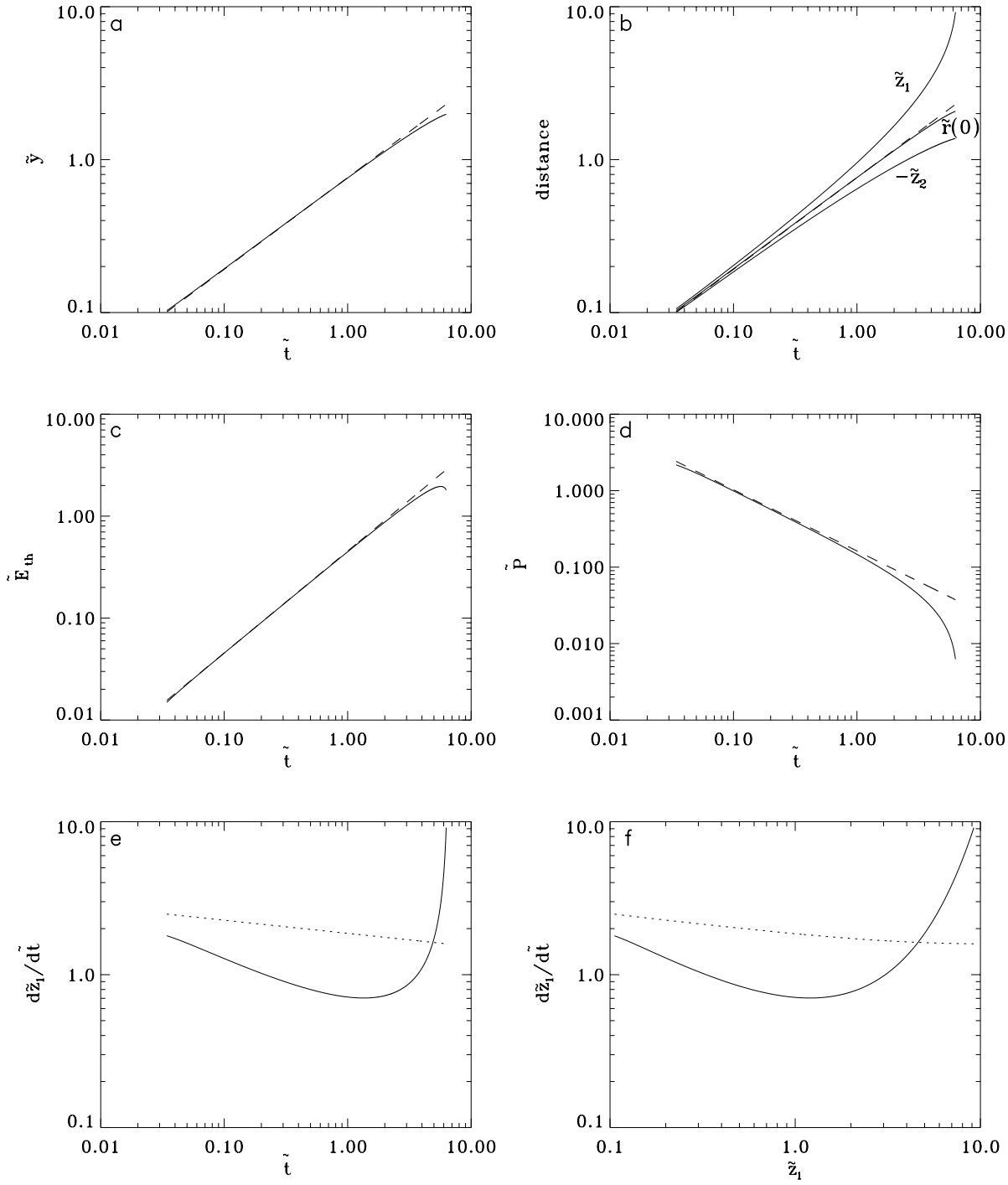

FIG. 10.—Time evolution of various dimensionless variables in the wind-blown Kompaneets solution (variables in *a*–*e* plotted vs. the dimensionless time $\tilde{t}$). (*a*) $\tilde{y}$. For comparison, the dimensionless solution for the radius of a spherical bubble in a uniform atmosphere, $\tilde{R}_s$, is shown with a dashed line. (*b*) Distance from the wind source to the shock front along various lines of sight: to the top of the bubble, $\tilde{z}_1$; along $z = 0$, $\tilde{r}(0)$; and to the bottom of the bubble, $-\tilde{z}_2$. Again, $\tilde{R}_s$ is shown with a dashed line. Together, (*a*) and (*b*) reveal the important feature $y \simeq r(0) \simeq R_s$. (*c*) Thermal energy $\tilde{E}_{th}$ within the bubble. The dashed line shows the time- evolution of $\tilde{E}_{th}$ in the spherical solution for a uniform atmosphere. (*d*) Pressure $\tilde{P}$ within the bubble. The dashed line shows the solution for a spherical bubble. (*e*) Velocity of the top of the bubble, $d\tilde{z}_1/d\tilde{t}$. The dotted line shows the internal sound speed $\tilde{c}_{s,i}$ for the parameters $n_0 = 1$ cm^{-3}, $L_0 = 3 \times 10^{37}$ ergs s^{-1}, and $H = 25$ pc. The Kompaneets approximation is expected to break down when $d\tilde{z}_1/d\tilde{t} > \tilde{c}_{s,i}$ ($\tilde{t} > 4.9$). (*f*) $d\tilde{z}_1/d\tilde{t}$ plotted vs. $\tilde{z}_1$; dotted line as in (*e*).

The evolution of the thermal energy $\tilde{E}_{th}(\tilde{t})$ is shown in Figure 10*c*. For comparison, the dimensionless spherical solution (from eq. [2]) is shown as a dashed line. Interestingly, $E_{th}(t)$ remains very close to the linear time-dependence of the spherical solution even after there is significant elongation of the bubble. This means that the term $Pd\Omega/dt$ in equation (A7) remains nearly constant even when the bubble is becoming elongated. At late times, $E_{th}(t)$ does fall significantly below the spherical expansion value and even begins to decrease. This decrease is due to the rapid expansion of the bubble in the late phases;

$d\Omega/dt$ increases without bound, approaching an infinite value at $\tilde{y} = 2$, causing the second term in equation (A7) to dominate the first, and making $dE_{\rm th}/dt$ negative. However, the Kompaneets approximation breaks down when the expansion speed exceeds the internal sound speed, so we cannot trust that the decrease of $E_{\rm th}(t)$ will occur in a more realistic model for this stage. Figure 10*d* shows the pressure $\tilde{P}$ versus $\tilde{t}$. Again, the dashed line shows the dimensionless spherical solution from equation (3). As with other variables, the pressure follows the spherical solution for much of the evolution, but it does drop significantly below it during the late stages. This stage coincides with the rapid expansion of the bubble, when one of the key assumptions of the Kompaneets approximation, uniform pressure within the bubble, begins to break down. Uniform pressure certainly cannot be maintained when the expansion speed exceeds the internal sound speed. A pressure gradient is then set up within the bubble. Hence the pressure at the base of the bubble, near the cluster, will not decrease to the values shown in Figure 10*d*.

We estimate the current pressure at the base by equating it to the mean pressure P at a time when rapid acceleration begins and the expansion speed approaches the internal sound speed. Beyond this critical time, we assume that the pressure at the base will not be able to readjust to a new value in the short time available. This gives us an estimate of the pressure at the base without going through the complexities of a full numerical solution of the hydrodynamic equations. We estimate the time at which the base pressure is frozen at the mean value by comparing dz_1/dt with the internal sound speed $c_{s,i} = (kT_b/\mu m_H)^{1/2}$. The bubble temperature T_b is estimated in Appendix B. Figures 10*e* and 10*f* show the speed of the top boundary $d\tilde{z}_1/d\tilde{t}$ versus $\tilde{t}$ and $\tilde{z}_1$, respectively; the latter gives an idea of where, rather than when, the acceleration phase occurs. Overplotted on both curves (*dashed lines*) is the internal sound speed $\tilde{c}_{s,i} = c_{s,i}/[v]$, where $[v]$ is the unit of velocity given in Table 1. The standard values $L_0 \simeq 3 \times 10^{37}$ ergs s^{-1} and $H \simeq 25$ pc are used to evaluate $[v]$, and n_0 is taken to be 1 cm^{-3}. We use dimensional values for L_0, H, and n_0 in this case, since the temperature depends implicitly on the thermal conductivity C within the bubble. Hence the sound speed depends on a fourth independent parameter and does not have a unique dimensionless value. Figures 10*e* and 10*f* show that the Kompaneets approximation breaks down after the top of the bubble departs from the $t^{-2/5}$ deceleration of the spherical solution and goes into the acceleration phase. The crossing of the two curves takes place at dimensionless time $\tilde{t} = 4.9$ for $n_0 = 1$ cm^{-3}, when the dimensionless pressure is $\tilde{P} \simeq 0.02$. Although this crossing would occur at a slightly later time and lower pressure, if we use a higher value for n_0, we use this dimensionless critical pressure in our analysis, since the combination of near-sonic velocity and very rapid acceleration make pressure readjustment unlikely after this time even for somewhat higher n_0 in the range 1–10 cm^{-3}. In § 3, we use the lower limit on the base pressure, $\tilde{P} \simeq 0.02$, as a parameter in our model for the ionization structure of the atmosphere.

APPENDIX B

SOME INTERIOR PROPERTIES OF THE W4 SUPERBUBBLE

B1. THE INTERIOR TEMPERATURE

The bubble temperature T_b is obtained from the model of Weaver et al. (1977). Their equation (37) for the interior temperature T in the bubble can be rewritten as

$$T = 63.6\left(\frac{L_0}{R_s}\right)^{2/7}\left(1 - \frac{r}{R_s}\right)^{1/5} \text{ K} . \tag{B1}$$

It is valid for $r < R_s$, where R_s is given by equation (1). Equation (B1) is obtained under the assumption of balance between the outward thermal conduction flux and the inward mechanical energy flux due to mass evaporation from the cool dense shell (see Weaver et al. 1977). Although our bubble is highly elongated, equation (B1) should give a reasonable estimate for the temperature near $z = 0$, since we find that the solution there is in many respects similar to the spherical solution. Normalizing to the standard wind luminosity and current radius $R_s \simeq r(z = 0) \simeq 50$ pc of the W4 superbubble, we find a central temperature (which is a representative value through most of a spherical bubble due to the weak radial dependence of eq. [B1])

$$T_b = 5 \times 10^6 \left(\frac{L_0}{3 \times 10^{37} \text{ ergs s}^{-1}}\right)^{2/7}\left(\frac{50 \text{ pc}}{R_s}\right)^{2/7} \text{ K} . \tag{B2}$$

B2. THE INNER SHOCK RADIUS

We estimate the inner shock front radius R_1 from the ram pressure of the free wind

$$P_w = \rho_w v_w^2 = \frac{\dot{M}}{4\pi r^2 v_w} v_w^2 = \frac{(2L_0 \dot{M})^{1/2}}{4\pi r^2} , \tag{B3}$$

where ρ_w is the wind density, v_w is the terminal velocity of the wind, $\dot{M}$ is the mass outflow rate, and the luminosity $L_0 = 1/2\dot{M}v_w^2$. Equating this to the pressure P_b inside the region of hot shocked gas yields a radius

$$R_1 = \frac{(2L_0 \dot{M})^{1/4}}{(4\pi P_b)^{1/2}} . \tag{B4}$$

Now the pressure in the bubble is written in dimensional form as

$$P_b = \tilde{P} \, (\rho_0 L_0^2 / H^4)^{1/3} , \tag{B5}$$

where $\tilde{P}$ is determined from the time evolution of the Kompaneets solution. In § A.2 we estimated that $\tilde{P} \simeq 0.02$ at the current epoch; hence using this as well as the most likely values $n_0 \simeq 10$ cm^{-3}, $L_0 \simeq 3 \times 10^{37}$ ergs s^{-1}, and $H \simeq 25$ pc for the W4 superbubble, we find that

$$P_b/k \simeq 1.1 \times 10^5 \text{ cm}^{-3} \text{ K} , \tag{B6}$$

where k is the Boltzmann constant. Using this value in equation (B4) with a total mass loss rate for the cluster stars $\dot{M} \simeq 10^{-5}$ $M_\odot$ yr^{-1} (see NTD), we find

$$R_1 \simeq 10 \text{ pc} . \tag{B7}$$

Hence the hot shocked gas occupies nearly the entire volume of the superbubble, and since $R_1 < H$, we are in retrospect justified in using spherical geometry to calculate R_1.

REFERENCES

Bisnovatyi-Kogan, G. S., Blinnikov, S. I., & Silich, S. A. 1989, Ap&SS, 154, 229
Bisnovatyi-Kogan, G. S., & Silich, S. A. 1995, Rev. Mod. Phys., 67, 661
Brinks, E., & Bajaja, E. 1986, A&A, 169, 14
Castor, J., McCray, R., & Weaver, R. 1975, ApJ, 200, L107
Dennison, B., Topasna, G. A., & Simonetti, J. H. 1997, ApJ, 474, L31 (DTS)
Deul, E. R., & den Hartog, R. H. 1990, A&A, 229, 362
Franco, J., Tenorio-Tagle, G., & Bodenheimer, P. 1990, ApJ, 349, 126
Heiles, C. 1979, ApJ, 229, 533
———. 1984, ApJS, 55, 585
Heyer, M. H., Brunt, C., Snell, R. L., Howe, J., Schloerb, F. P., & Carpenter, J. M. 1998, ApJS, 115, 241
Heyer, M. H., & Terebey, S. 1998, ApJ, 502, 265
Heyer, M. H., et al. 1996, ApJ, 464, L175
Komljenovic, P. T., Basu, S., & Johnstone, D. 1999, in ASP Conf. Ser., New Perspectives on the Interstellar Medium, ed. A. R. Taylor, T. L. Landecker, & G. Joncas (San Francisco: ASP), 168, 299
Kompaneets, A. S. 1960, Soviet Phys. Dokl., 5, 46
Korycansky, D. G. 1992, ApJ, 398, 184
Kulkarni, S. R., & Heiles, C. 1987, in Interstellar Processes, ed. D. J. Hollenbach & H. A. Thronson, Jr. (Dordrecht: Reidel), 87
MacLow, M.-M., & McCray, R. 1988, ApJ, 324, 776
MacLow, M.-M., McCray, R., & Norman, M. L. 1989, ApJ, 337, 141
Massey, P., Johnson, K. E., & DeGioia-Eastwood, K. 1995, ApJ, 454, 151
McCray, R., & Kafatos, M. 1987, ApJ, 317, 190
McKee, C. F., Van Buren, D., & Lazareff, B. 1984, ApJ, 278, L115
Norman, C. A., & Ikeuchi, S. 1989, ApJ, 345, 372
Normandeau, M., Taylor, A. R., & Dewdney, P. E. 1996, Nature, 380, 687 (NTD)
———. 1997, ApJS, 108, 279 (NTD)
Puche, D., Westpfahl, D., Brinks, E., & Roy, J.-R. 1992, AJ, 103, 1841
Reynolds, R. J. 1989, ApJ, 339, L29
———. 1991, ApJ, 372, L17
Schiano, A. V. R. 1985, ApJ, 299, 24
Shapiro, P. R. 1979, ApJ, 233, 831
Spitzer, L., Jr. 1978, Physical Processes in the Interstellar Medium (New York: Wiley)
Stone, J. M., & Norman, M. L. 1992, ApJ, 389, 297
Tenorio-Tagle, G. 1982, in Regions of Recent Star Formation, ed. R. S. Roger & P. E. Dewdney (Dordrecht: Reidel), 1
Tenorio-Tagle, G., Rozyczka, M., & Bodenheimer, P. 1990, A&A, 237, 207
Tomisaka, K. 1992, PASJ, 44, 177
———. 1998, MNRAS, 298, 797
Tomisaka, K., & Ikeuchi, S. 1986, PASJ, 38, 697
Weaver, R., McCray, R., Castor, J., Shapiro, P., & Moore, R. 1977, ApJ, 218, 377